Available online at www.sciencedirect.com
SCIENCE DIRECT
Coordination Chemistry Reviews 250 (2006) 1471–1496
COORDINATION CHEMISTRY REVIEWS
www.elsevier.com/locate/ccr

Review

Photophysical properties of metal-mediated assemblies of porphyrins

Franco Scandola [a,b,c,*], Claudio Chiorboli [b,c], Anna Prodi [a], Elisabetta Iengo [d], Enzo Alessio [d,**]

[a] *Dipartimento di Chimica, Università di Ferrara, 44100 Ferrara, Italy*
[b] *INSTM, Sezione di Ferrara, 44100 Ferrara, Italy*
[c] *ISOF-CNR, Sezione di Ferrara, 44100 Ferrara, Italy*
[d] *Dipartimento di Scienze Chimiche, Università di Trieste, 34127 Trieste, Italy*

Received 18 November 2005; accepted 24 January 2006
Available online 14 March 2006

Contents

Abstract

The metal-driven construction of multi-porphyrin assemblies, which exploits the formation of coordination bonds between peripheral basic site(s) on the porphyrins and metal centers, has recently allowed the design and preparation of sophisticated supramolecular architectures whose complexity and function begin to approach the properties of naturally occurring systems. Within this framework, *meso*-pyridyl/phenyl porphyrins (PyPs), or strictly related chromophores, can provide geometrically well-defined connections to as many as four metal centers by coordination of the pyridyl peripheral groups. Several discrete assemblies of various nuclearities, in which the pyridylporphyrins are linkers binding metalloporphyrins and/or coordination compounds, have been constructed in recent years. In this review, we summarize recent work from our laboratories on metal-mediated

Abbreviations: TPP, tetraphenylporphyrin; OEP, octaethylporphyrin; 4′MPyP, 5-(4′pyridyl)-10,15,20-triphenylporphyrin; 3′MPyP, 5-(3′pyridyl)-10,15,20-triphenylporphyrin; 4′-*cis*DPyP, 5,10-bis(4pyridyl)-15,20-diphenylporphyrin; 3′-*cis*DPyP, 5,10-bis(3′pyridyl)-15,20-diphenylporphyrin; 4′-*trans*DPyP, 5,15-bis(4′pyridyl)-10,20-diphenylporphyrin; 4′-*trans*DPyP-npm, 5,15-bis(4′-pyridyl)-2,8,12,18-tetranormalpropyl-3,7,13,17-tetramethylporphyrin; 4′TPyP, 5,10,15,20-tetra(4′pyridyl)porphyrin; 3′TPyP, 5,10,15,20-tetra(3′pyridyl)porphyrin; DPyPBI, *N*,*N*′-di(4-pyridyl)-1,6,7,12-tetra(4-*tert*-butylphenoxy)perylene-3,4:9,10-tetracarboxylic acid bisimide; pyz, pyrazine; pym, pyrimidine; dppp, 1,3-bis(diphenylphosphino)propane; OTf, triflate

* Corresponding author. Tel.: +39 0532291160; fax: +39 0532240709.
** Corresponding author.
E-mail addresses: snf@unife.it (F. Scandola), alessi@mail.univ.trieste.it (E. Alessio).

0010-8545/$ – see front matter
doi:10.1016/j.ccr.2006.01.019

multi-porphyrin assemblies and their photophysical properties. The review is organized as follows: after a brief summary of relevant concepts on energy and electron transfer processes and their implications in charge separation and the antenna effect (Section 2), the main assembling strategies leading to side-to-face and metal-mediated assemblies are synthetically reviewed (Section 3). The photophysical studies leading to the identification and kinetic characterization of the photoinduced energy and/or electron transfer processes within the supramolecular structures are surveyed in Section 4.

Keywords: Multi-porphyrin assemblies; Metal-mediated assemblies; Pyridylporphyrins; Photo-induced processes; Electronic energy transfer; Electron transfer; Antenna effect

1. Introduction

According to the paradigm of supramolecular photochemistry [1], suitable assemblies of molecular components (supramolecular systems) can be designed to emulate, at the molecular level, *light-induced functions* typical of biological systems or of artificial macroscopic electronic devices. Thus, synthetic supramolecular architectures can in principle be designed to mimic, e.g., the light-harvesting complexes and reaction centers of natural photosynthesis, or to perform as molecular switches, optical memories, logic gates, shift registers, optoelectronic gates, fluorescent sensors, light-driven molecular machines, etc. The ultimate extension of this concept would be the construction, in a bottom-up approach, of optoelectronic devices from molecules (molecular photonics).

Among many interesting light-induced functions, those inspired by natural photosynthesis have attracted special attention. In fact, as a result of extensive spectroscopic studies and detailed structural determinations, the *photoinduced charge separation* taking place in the reaction centers [2] and the *antenna effect* carried out by the light-harvesting units [3] are now understood in great detail. On the other hand, artificial supramolecular systems mimicking the photoinduced charge separation [4] and the antenna effect [5] are the subject of continuing research activity, fostered by the problem of artificial solar energy conversion. In many of these artificial systems, porphyrin (and/or metalloporphyrin) units play a major role. In fact, aside from their chemical resemblance to the chlorophylls of the natural systems, porphyrins can be considered as ideal components for the construction of artificial supramolecular systems because of several appealing features: rigid, planar geometries; high stability; intense electronic absorption bands in the visible region; relatively long fluorescence decay time; facile tunability of their optical and redox properties by metalation/functionalization; availability of a variety of synthetic strategies for supramolecular organization.

Particularly interesting porphyrin arrays are those based on *pyridylporphyrins*, i.e. porphyrins carrying a number ($n = 1$–4) of pyridyl substituents at the *meso* positions (with the remaining 4-*n* positions occupied by aryl groups, or bearing alkyl chains at the β positions). With these chromophores, the coordinating ability of the peripheral pyridyl groups can be used for assembling purposes. In fact, a great variety of *metal-bridged arrays* have been obtained by coordination of pyridylporphyrins to appropriate metal complex fragments [6–8]. On the other hand, structurally interesting *side-to-face arrays* can be obtained by axial coordination between pyridylporphyrins and metalloporphyrins [9,10].

In this review, we summarize recent work from our laboratories on metal-mediated multi-porphyrin assemblies and their photophysical properties. The review is organized as follows: after a brief summary of relevant concepts on energy and electron transfer processes and their implications in charge separation and the antenna effect (Section 2), the main assembling strategies leading to side-to-face and metal-mediated assemblies are synthetically reviewed (Section 3). The photophysical studies leading to the identification and kinetic characterization of the photoinduced energy and electron transfer processes within the supramolecular structures are surveyed in Section 4.

2. Photoinduced processes in supramolecular systems

In supramolecular systems, the most important intercomponent processes taking place following light excitation are *electronic energy transfer* and *photoinduced electron transfer*. In this section, some basic concepts about these processes are briefly summarized. The supramolecular system is schematized here as a simple "dyad", D–B–A, where two molecular components D and A are connected via an appropriate chemical linker B.

2.1. Energy transfer

In a supramolecular system electronic energy transfer (Fig. 1) can be viewed as a radiationless transition between two "local" electronically excited states of the system (Eq. (1))

$$^{*}\text{D–B–A} \rightarrow \text{D–B–}^{*}\text{A} \quad (1)$$

The rate constant (k_{en}) for the energy transfer process is thus given by a "golden rule" expression (Eq. (2))

$$k_{en} = \frac{4\pi}{h}(H_{if}^{en})^2 \text{FCWD}^{en} \quad (2)$$

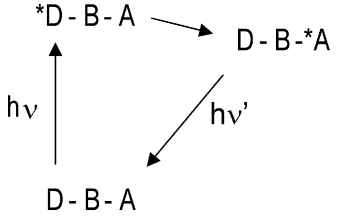

Fig. 1. Electronic energy transfer in a covalently linked dyad.

In Eq. (2) H_{if}^{en} is the electronic coupling between the two excited states interconverted by the energy transfer process and $FCWD^{en}$ is an appropriate Franck–Condon factor.

The Franck–Condon factor [11–13] is a thermally averaged sum of vibrational overlap integrals, representing the distribution of the transition probability over several isoenergetic "virtual transitions" (from *D to D, and from A to *A) in the two molecular components. In terms of experimental quantities, it is proportional to a spectral overlap integral J (Eq. (3)) between

$$J = \int_0^\infty F_A(\bar{\nu})\varepsilon_B \, d\bar{\nu} \tag{3}$$

the emission of the donor and the absorption of the acceptor. Experimental studies of Franck–Condon effects in energy transfer processes have been carried out [14–15].

The electronic factor H_{if}^{en} is a two-electron matrix element involving the HOMOs and LUMOs of the energy-donor and energy-acceptor centers. Following standard arguments [16], this factor can be split into additive *coulombic* and *exchange* terms. The two terms depend differently on various parameters of the system (spin of ground and excited states, donor–acceptor distance, etc.). This leads to the identification of two main energy transfer mechanisms, as pictorially represented in Fig. 2.

The *coulombic* (also called "resonance", "dipole–dipole", or "Förster-type") mechanism [17] is a long-range mechanism that does not require physical contact between donor and acceptor. The most important contribution within the coulombic interaction is the dipole–dipole term, that obeys the same selection rules as the corresponding electric dipole transitions of the two partners. Therefore, coulombic energy transfer is expected to be efficient in systems in which the radiative transitions connecting the ground and the excited state of each partner have high oscillator strength. The relationship between the rate constant for coulombic energy transfer and the spectroscopic and photophysical properties of the two molecular components is given by the classical Förster formula (Eq. (4)),

$$k_{en}^{coul} = 1.25 \times 10^{17} \frac{\Phi_A}{n^4 \tau_A r_{AB}^6} \int_0^\infty F_A(\bar{\nu})\varepsilon_B \frac{d\bar{\nu}}{\bar{\nu}^4} \tag{4}$$

where Φ_A is the quantum yield of donor emission, n the solvent refractive index, τ_A the lifetime of the donor emission, r_{AB} the distance (in nm) between donor and acceptor, F_A the emission spectrum of the donor (in wavenumbers and normalized to unity), and ε_B is the decadic molar extinction coefficient of the acceptor. With a good spectral overlap integral and appropriate photophysical parameters, the $(1/r_{AB}^6)$ distance dependence allows energy transfer to occur efficiently over distances largely exceeding the molecular diameters (e.g. 50 Å). Coulombic energy transfer is therefore also called "long-range energy transfer". The typical example of efficient coulombic mechanism is that of singlet–singlet energy transfer (Eq. (5)).

$$^*D(S_1)\text{–}B\text{–}A(S_0) \rightarrow D(S_0)\text{–}B\text{–}^*A(S_1) \tag{5}$$

The *exchange* (also called "Dexter-type") mechanism [17] is a short-range mechanism that requires orbital overlap, and therefore physical contact, between donor and acceptor. The exchange interaction can be visualized as the simultaneous exchange of two electrons between the donor and the acceptor (Fig. 2). The spin selection rules for this type of mechanism reflect the need to obey spin conservation in the reacting pair as a whole. Therefore, the exchange mechanism can be operative not only with spin-allowed states (as, e.g. in Eq. (5)) but also in many cases in which the excited states involved are spin-forbidden in the spectroscopic sense. Thus, the typical example of efficient exchange mechanism is that of triplet–triplet energy transfer (Eq. (6)).

$$^*D(T_1)\text{–}B\text{–}A(S_0) \rightarrow D(S_0)\text{–}B\text{–}^*A(T_1) \tag{6}$$

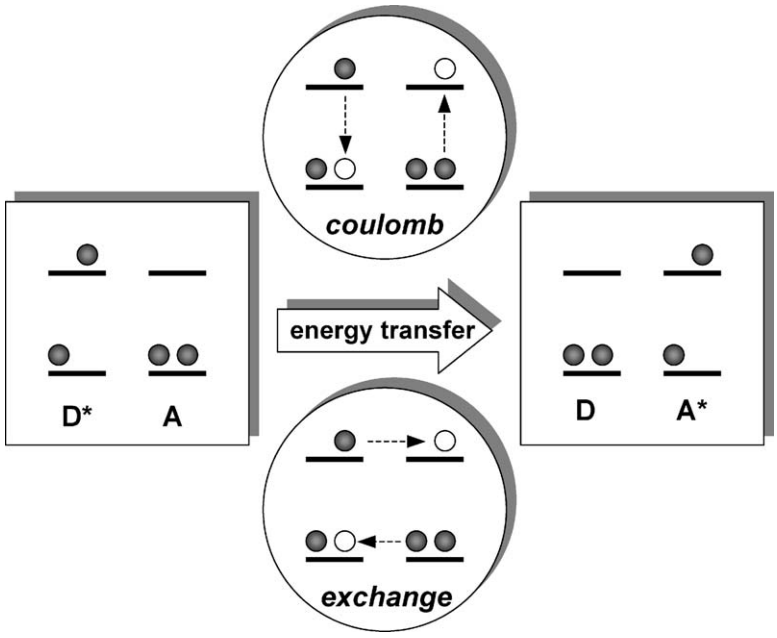

Fig. 2. Coulombic and exchange mechanisms for electronic energy transfer. Schematic representation in terms of electron transitions between frontier orbitals.

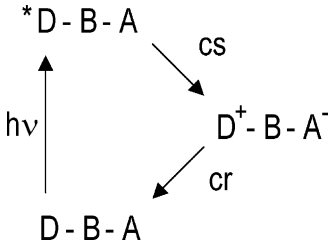

Fig. 3. Photoinduced electron transfer in a covalently linked dyad.

The rate constant of exchange energy transfer is expected to be sensitive to the nature of the linker B connecting the donor and acceptor molecular components, as the donor–acceptor exchange interaction can be effectively mediated by bridge-localized orbitals. With long, modular bridges, the exchange interaction is expected to fall off exponentially with through-bond distance, or with number of intervening units in the bridge [18–20]. Experimental correlations between the distance dependence of exchange energy transfer and of electron/hole transfer processes support the simple picture of exchange energy transfer as a "simultaneous double electron transfer" [21].

2.2. Electron transfer

A possible scheme for photoinduced electron transfer is shown in Fig. 3 (alternatively, a similar scheme in which the photoexcited molecular component plays the role of acceptor could be considered). In the absence of chemical complications, the primary products are expected to undergo back electron transfer to regenerate the starting ground-state system. The photoinduced forward process and the back reaction are often called *charge separation* (cs) and *charge recombination* (cr), respectively.

For a supramolecular system, the driving force of an excited-state electron transfer process can be easily calculated on the basis of electrochemical and spectroscopic data on the isolated molecular components, with the appropriate corrections for electrostatic work terms [22]. As far as kinetics are concerned, electron transfer processes can be described in terms of quantum mechanical [23–25] or classical [26–30] models. From a quantum mechanical viewpoint, both photoinduced electron transfer (Eq. (7)) and charge recombination (Eq. (8)) can be viewed as

$$D^*\text{–B–A} \rightarrow D^+\text{–B–A}^- \tag{7}$$

$$D^+\text{–B–A}^- \rightarrow D\text{–B–A} \tag{8}$$

examples of radiationless transitions between different, weakly interacting electronic states of the supermolecule D–B–A. The probabilities of such processes are given by a "golden rule" expression of the type (Eq. (9)) [26–29],

$$k_{el} = \frac{4\pi}{h} H_{if}^{el2} \mathrm{FCWD}^{el} \tag{9}$$

in which H_{if}^{el} is the electronic coupling between the two states interconverted by the electron transfer process and FCWD^{el} is a thermally averaged vibrational Franck–Condon factor ("Franck–Condon weighted density of states").

In covalently linked D–B–A dyads, the donor–acceptor electronic coupling is effectively mediated by the bridging group B (*through-bond* mechanism) [30,31]. Through-bond electronic coupling can be conveniently accounted for in terms of superexchange [30,32–38]. The essential notion is that, although direct interaction between the initial and final states of the electron transfer process is negligible, indirect coupling takes place by mixing with high-energy states of charge transfer character (often called "virtual states") involving the bridge. Thus, low-energy LUMO (easily reducible) and/or high-energy HOMO (easily oxidizable) bridges are good electron transfer superexchange mediators. For long, modular bridges, not only the chemical nature, but also the length is relevant to the electron transfer rate. In this case, the superexchange model predicts an exponential dependence of H_{if}^{el} on the number of modular units [33,37,38], and thus of the donor–acceptor distance (Eq. (10)),

$$H_{if}^{el} = H_{if}^{el}(0) \exp\left[-\frac{\beta}{2}(r_{AB} - r_0)\right] \tag{10}$$

where r_{AB} is the donor–acceptor distance, $H_{if}^{el}(0)$ the interaction at "contact" distance r_0, and β is an attenuation parameter (also named "damping factor") representing the intrinsic electron-mediating ("conducting") ability of the bridge. The predicted exponential decay of the electronic coupling has been verified in several homogeneous series of dyads containing modular organic bridges of variable length [37,38].

The FCWD^{el} term of Eq. (5) (often referred to as the "nuclear factor" of the rate constant) is a thermally averaged Franck–Condon factor connecting the initial and final states. It contains a sum of overlap integrals between the isoenergetic nuclear wavefunctions of reactant and product. The nuclear wavefunctions include both (inner) vibrational modes and (outer) solvent reorganizational modes. The summation is made over the initial levels of the reactant, suitably weighted for their Boltzmann population. The expression of FCWD^{el}, which is quite complicated in a general case [26], becomes relatively simple in idealized situations. For example, in a simple approximation in which the solvent modes (average frequency, ν_o) are thermally excited and treated classically ($h\nu_o \ll kT_B$), and the internal vibrations (average frequency, ν_i) are frozen and treated quantum mechanically ($k_B T \ll h\nu_i$), and a single internal mode is assumed to be involved, the FCWD^{el} term is given by Eq. (11) [26,28]

$$\mathrm{FCWD}^{el} = \left(\frac{1}{4\pi\lambda_o k_B T}\right)^{1/2} \sum_m S^m \frac{e^{-S}}{m!} \exp \times \left[-\frac{(\Delta G^\circ + \lambda_o + mh\nu_i)^2}{4\lambda_o k_B T}\right] \tag{11}$$

$$S = \frac{\lambda_i}{h\nu_i} \tag{12}$$

In Eq. (11), the summation extends over m, the number of quanta of the inner vibrational mode in the product state, ΔG° is the thermodynamic driving force of the process, S is defined by

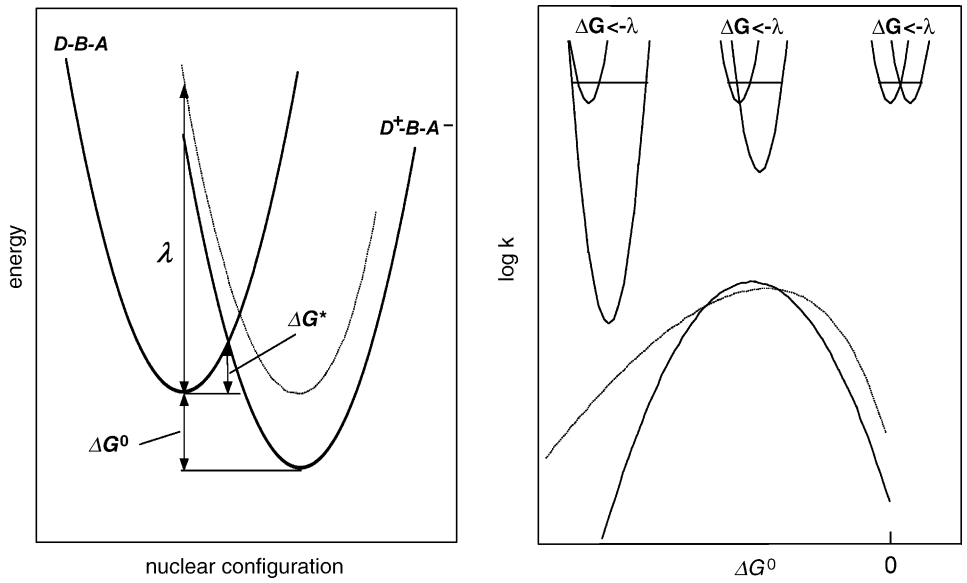

Fig. 4. Left: Marcus model and kinetic parameters for an electron transfer reaction. Right: free-energy dependence of electron transfer rate (continuous line, Eq. (15); dotted line: Eq. (11)) in the "normal" (right), "activationless" (center), and "inverted" (left) kinetic regimes.

Eq. (12), and, λ_o is the outer-sphere (solvent) reorganizational energy, given in its simplest form [23–25] by Eq. (13),

$$\lambda_o = e^2 \left(\frac{1}{2r_A} + \frac{1}{2r_B} - \frac{1}{r_{AB}} \right) \left(\frac{1}{D_{op}} - \frac{1}{D_s} \right) \quad (13)$$

where e is the electron charge, D_{op} and D_s the optical and static dielectric constants of the solvent, r_A and r_B the radii of the two molecular components, and r_{AB} is the intercomponent distance. In Eq. (12), λ_i is the inner-sphere (vibrational) reorganizational energy given, in the single mode approximation, by Eq. (14),

$$\lambda_i = \frac{1}{2} k \, \Delta Q^2 \quad (14)$$

where k is an average force constant and ΔQ is the change in equilibrium geometry along the vibrational mode considered.

It can be shown [24] that in the high temperature limit (i.e. when $h\nu < k_B T$ for all relevant nuclear modes, a reasonable approximation for many practical cases at room temperature), the nuclear factor takes the simple form (Eq. (15)):

$$\text{FCWD} = \left(\frac{1}{4\pi\lambda k_B T} \right)^{1/2} \exp \left[-\frac{(\Delta G^\circ + \lambda)^2}{4\lambda k_B T} \right] \quad (15)$$

where $\lambda = \lambda_i + \lambda_o$. The exponential term of Eq. (15) is the same as that predicted by the classical Marcus model [23–25], based on parabolic energy curves for reactants and products such as those of Fig. 4, in which the activation free energy is that required for going from the equilibrium geometry of the reactants to the crossing point. Both classical (Eq. (15)) and quantum mechanical (Eq. (11)) models contain an important prediction, namely that three typical kinetic regimes exist, depending on the driving force of the electron transfer reaction: (i) a "normal" regime for small driving forces ($-\lambda < \Delta G^\circ < 0$) in which the electron transfer process is thermally activated and is favored by an increase in driving force; (ii) an "activationless" situation ($-\lambda \approx \Delta G^\circ$) in which very small changes in rate are obtained by changing the driving force; (iii) an "inverted" regime for strongly exoergonic reactions ($-\lambda > \Delta G^\circ$) in which the electron transfer process *slows down* with increasing driving force. Thus, an increase of λ slows down the process in the normal regime, but accelerates it in the inverted regime. The three kinetic regimes are schematically shown, in terms of classical Marcus' parabolae, in Fig. 4. The main difference between the classical (Eq. (15)) and the quantum mechanical expression (Eq. (11)) lies in the type of quantitative free-energy dependence predicted for $\ln k_{el}$ in the inverted region (Fig. 4), respectively, parabolic [23] and linear (so-called "energy-gap-law") [26]. Experimental evidence for the inverted region in electron transfer kinetics has been obtained in systematic studies of homogeneous series of reactions [39,40].

2.3. Light-induced functions

Energy and electron transfer are key steps of two important light-induced functions of natural photosynthesis: light harvesting (antenna effect) and photoinduced charge separation. In the natural photosynthetic systems, these functions are performed by extremely complex, highly sophisticated supramolecular structures (light harvesting complexes, reaction centers). The basic principles underlying such functions are, however, relatively simple and can be illustrated in a schematic way as follows. Generally speaking, an artificial antenna is a multicomponent system (Fig. 5) in which several chromophoric molecular units absorb the incident light and funnel the excitation energy to a common acceptor component where the energy can be ultimately utilized (as emitted light or to effect a useful chemical reaction). To this aim, two features should be implemented in the supramolecular array: (i) energy should be rapidly and randomly transferred between iso-energetic chromophoric units and (ii) small energy gradients between chromophores should be used

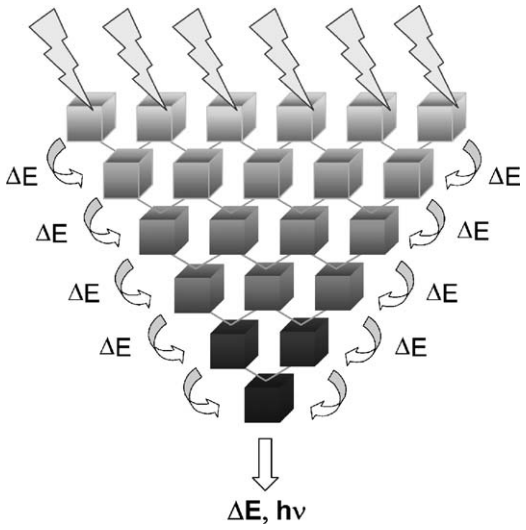

Fig. 5. Schematic representation of an artificial antenna system.

to direct the energy flow towards the utilization site. To match these requirements, ideal chromophores should have transitions of high oscillator strength (high ε_B and Φ_A/τ_A in Eq. (4)) and small excited-state distortion (small Stokes shifts) so as to give large J values (Eq. (3)) with minimum driving force. Porphyrins, with their strong π–π^* transitions and their rigid planar structure meet these requirements to a high degree. This justifies their wide use as building blocks for the design and synthesis of artificial antenna model systems [5].

In simple dyads, fast charge recombination is expected to follow photoinduced electron transfer (Fig. 3). As shown by the reaction centers of natural photosynthesis, the winning strategy to overcome the energy wasting charge recombination is to introduce further molecular components and perform a *stepwise charge separation* process. The minimal set to illustrate this point is a triad (Fig. 6).

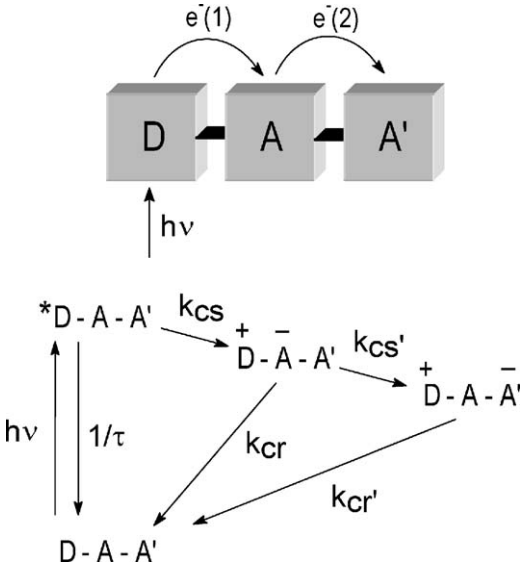

Fig. 6. Schematic representation of a charge separating triad.

Among various possible triad schemes, we use as an example that of Fig. 6, in which two consecutive electron transfer steps take place: (1) from the excited chromophore, D^*, to a primary acceptor molecular component, A (cs); (2) from the primary acceptor to a secondary acceptor component, A′ (cs′). The yield of charge separation is given by Eq. (16),

$$\Phi_{cs} = \frac{k_{cs}}{k_{cs} + (1/\tau)} \frac{k_{cs'}}{k_{cs'} + k_{cr}} \tag{16}$$

while the lifetime of the charge separated state is simply $1/k_{cr'}$. Of the two terms in Eq. (16), the first one (efficiency of quenching of the excited chromophore) is maximized by long-lived excited states and fast electron transfer. Often, the key to the overall efficiency lies in the second term of Eq. (16), i.e. in the competition between primary charge recombination, k_{cr}, and secondary electron transfer process, $k_{cs'}$. This term can be maximized if $k_{cs'}$ lies in the "normal" and k_{cr} in the "inverted" Marcus free energy regime (Fig. 4). If the charge separation is used for energy conversion purposes, a further requirement is that the energy loss in the two consecutive electron transfer steps is as small as possible. In order to meet all of the above requirements, the molecular components of a triad should have an as small as possible reorganizational energy (λ in Eq. (15)). From this viewpoint, the porphyrins are ideally suited in terms of their large size (small λ_o in Eq. (13)) and highly delocalized electronic structure (small distortion upon reduction/oxidation, ΔQ in Eq. (14)). Several triads (as well as more complex systems, tetrads, pentads, etc.) have been successfully developed [4], many of which involve porphyrins as chromophores.

3. Metal-mediated assemblies of porphyrins

For the construction of metal-mediated multichromophore assemblies we have mainly exploited *meso*-pyridyl/phenylporphyrins (PyPs), a class of *electron-donor* building blocks which can provide geometrically well defined connections to as many as four metal centers by coordination of the peripheral *meso* pyridyl groups (Fig. 7).

The pyridyl nitrogen atom(s) of PyPs can be either in 4′ or in 3′ position [41]. With 4′PyPs the coordination bonds are established in the plane of the porphyrin, along the *meso* bond axes; with 3′PyPs instead, since the *meso* pyridyl rings are tilted, the coordination bonds are directed out of the plane of the chromophore (Chart 1).

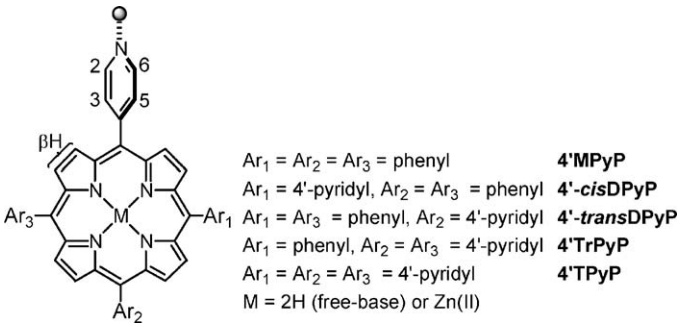

Fig. 7. Schematic drawing of 4′PyPs with numbering scheme; grey circle symbolizes an external metal center.

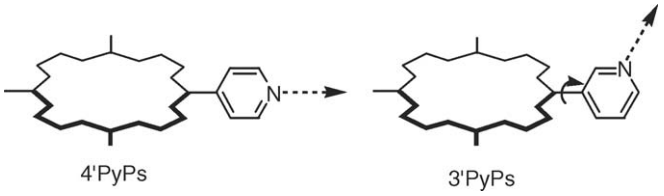

Chart 1.

The change in the position of the nitrogen atom in the pyridyl ring(s) is expected to induce major changes in the geometry of the resulting metal-mediated supramolecular systems, even though these changes are not easily predictable a priori.

The *electron-acceptor* building blocks, i.e. the metal centers, may either be located in the core of another porphyrin or belong to a coordination compound. When porphyrins bearing appended ligands bind to metallo-porphyrins, assemblies of axially connected chromophores are generated (side-to-face assemblies) (Fig. 8).

In metalloporphyrins the number of coordination axial sites that can be exploited, usually one or two, their lability as well as the affinity toward different donor atoms can be fine-tuned by changing the nature and the oxidation state of the metal center. Moreover, the electronic structure (electron-acceptor properties of the metal center), and the access to the porphyrin core, can be designed by means of well-planned peripheral substitutions either at the β-pyrrole or *meso* position(s).

The alternative synthetic strategy towards metal-mediated supramolecular assemblies of chromophores, which exploits the formation of coordination bonds between peripheral donor sites on the porphyrins and external metal centers (either naked ions or coordination compounds), is extremely convenient and versatile. In particular, when the design of robust three-dimensional structures with precise size and shape is of interest, the use of coordination compounds as structural units has proved to be very efficient [6]. A large and diverse number of transition-metal coordination geometries can be exploited in the construction of elaborate assemblies, giving access to different topologies rather difficult to obtain with the classical synthetic methods. An appropriate choice of the ancillary ligands allows to fine-tune the charge and polarity (and thus solubility) of the final adduct and to introduce additional functionalities (e.g. chirality). In addition, also the metallic connectors, if appropriate coordination complexes are chosen, may introduce useful photophysical properties into the assemblies.

Examples of multichromophore systems prepared by us with these two synthetic approaches, that lead to very different architectures, will be treated separately in the following sections. A common feature of these oligomeric systems is that their visible spectrum matches very closely the sum of the spectra of the single monomeric components, indicating weak mutual perturbation of the chromophoric units. This additive behavior indicates that these arrays are true supramolecular systems, i.e. weakly interacting multi-component systems in which the energy levels of each chromophore are substantially unperturbed by inter-component interactions.

3.1. Side-to-face assemblies of chromophores

We mainly exploited zinc-porphyrins and Ru(CO)-porphyrins: both are neutral and have only one axial site available for coordination (the carbonyl ligand in Ru(II)(CO)-porphyrins is very tightly bound and not easily displaced) and a good affinity for pyridyl ligands. However, while the Zn(II)-porphyrin–*N*-(pyridyl) interaction is intrinsically weak (association constant ca. $10^3\,M^{-1}$) and relatively labile, stronger and more inert bonds are obtained for Ru(II)(CO)-porphyrins and N-heterocycles. As a consequence, in the absence of cooperativity (see below), the assemblies based on coordination to zinc-porphyrins are not sufficiently stable at photophysical concentrations (typically $10^{-6}\,M$) and we preferred coordination to ruthenium porphyrins.

We found that treatment of PyPs with the required amount of [Ru(TPP)(CO)(EtOH)] in chloroform at room temperature leads rapidly and quantitatively (assessed by

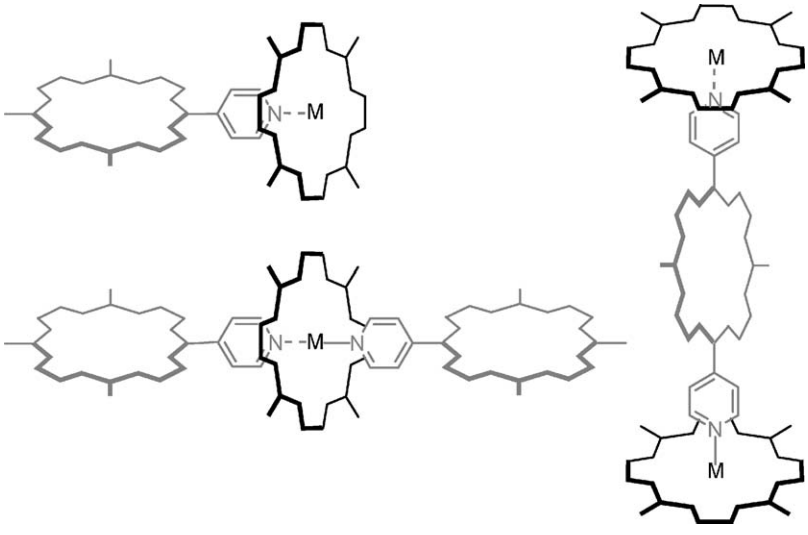

Fig. 8. Schematic examples of discrete side-to-face multiporphyrin assemblies that can be obtained with 4′PyPs.

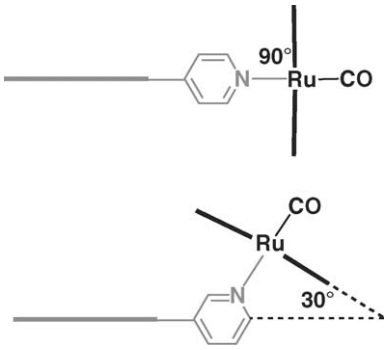

Chart 2.

^{1}H NMR) to the corresponding side-to-face assembly (from the dimer [Ru(TPP)(CO)(MPyP)] to the pentamer [(TPyP){Ru(TPP)(CO)}$_4$]) in which all the peripheral pyridyl groups of the central PyP are axially bound to a ruthenium-porphyrin [9,42]. The products are more soluble than the original PyP. Derivatives (in which the central PyP is zincated) (i.e., [Ru(TPP)(CO)(Zn·MPyP)] and [(Zn·TPyP){Ru(TPP)(CO)}$_4$]) were best synthesized by treatment of the oligomers with an excess of zinc acetate in $CHCl_3$/MeOH mixtures. While 4′PyPs led to assemblies of perpendicularly linked porphyrins, 3′PyPs yielded the corresponding tilted adducts.

The solution structures of the assemblies were assessed by ^{1}H NMR spectroscopy; signal assignments were supported by 2D H–H COSY and NOESY experiments. Pyridyl signals were always sharp; no exchange between coordinated and free PyPs was observed at NMR concentrations. Signal integration revealed adduct stoichiometry, while the pyrrole resonances of PyPs were characteristic of the geometry. A common feature in the NMR spectra of axially ligated porphyrin aggregates is the dramatic upfield shift of the resonances of the central chromophore induced by the (cumulative) anisotropic shielding effect of the peripheral porphyrin(s). The NMR data, through chemical shift and symmetry arguments, also indicated that at room temperature all the *meso* six-membered rings experience hindered rotation about the C(*meso*)–C(ring) bond and lie essentially perpendicular to the mean plane of the corresponding porphyrin. Therefore, in solution the dihedral angles between the mean plane of the central PyP and those of the peripheral Ru(TPP)(CO) units, on average, are very likely close to the ideal values of 90° (4′PyPs) and 30° (3′PyP), respectively (Chart 2).

The X-ray structure of the dimeric adduct [Ru(TPP)(CO)(3′MPyP)] (**1**) established that in the solid state the dihedral angle between the mean plane of 3′MPyP and that of TPP is very close to 40° (compared to ca. 81° in [Ru(OEP)(CO)(4′MPyP)]) [10a] (Fig. 9).

We mainly focused on the two symmetrical pentameric side-to-face assemblies obtained with 4′TPyP and 3′TPyP, respectively. The *orthogonal* pentamer, [(4′TPyP){Ru(TPP)(CO)}$_4$] (**2**), has a predicted shape best described as two attached open-ended square boxes sharing a common bottom (4′TPyP) and four Ru(TPP)(CO) units as walls (Fig. 10).

Assuming normal bond distances and angles, a cavity width of ca. 20 Å at the base is estimated. X-ray investigation performed on [(Zn·3′TPyP){Ru(TPP)(CO)}$_4$] (**3Zn**) allowed us to establish that the *tilted* analogues **3** and **3Zn** have a very compact and symmetrical structure; the ruthenium porphyrins lie alternatively above and below the mean plane of the central Zn·3′TPyP unit. The particularly simple ^{1}H NMR spectrum of the pentamer indicated that a symmetrical arrangement of the four Ru(TPP)(CO) units around 3′TPyP, very likely similar to that found in the solid state, is preserved also in solution. In ^{1}H NMR spectra of **2/2Zn** and **3/3Zn** all phenyl rings are equivalent, indicating free rotation of Ru(TPP) units about the Ru–N(py) bonds.

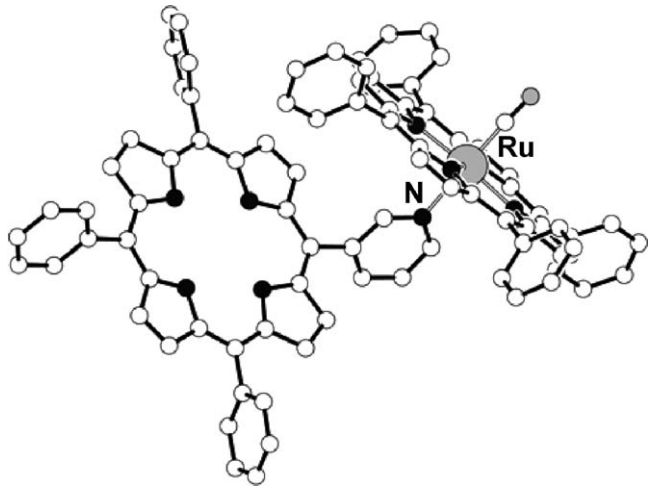

Fig. 9. X-ray structure of [Ru(TPP)(CO)(3′MPyP)] (**1**) (adapted from Ref. [9b]).

We also made bisporphyrin sandwich assemblies by connecting two Ru(TPP)(CO) units through *metal-containing ligands* with a *trans* geometry, such as [{*trans,trans,trans-*

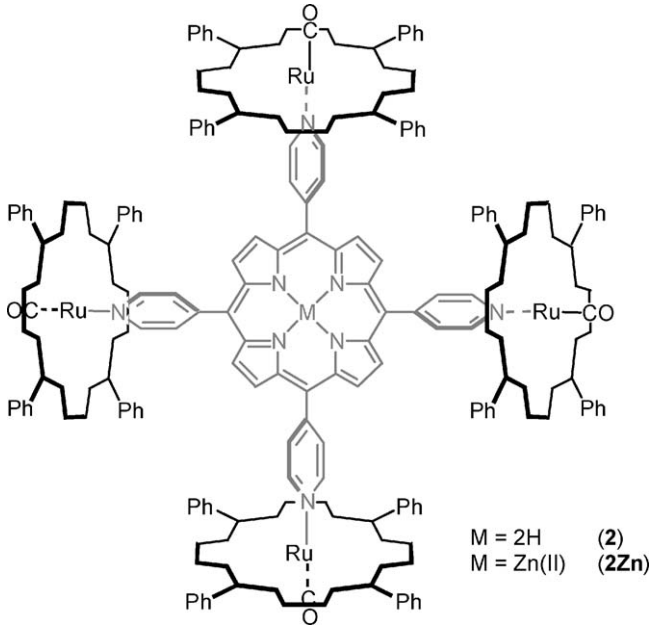

Fig. 10. Schematic drawing of the *orthogonal* pentamer [(4′TPyP){Ru(TPP)(CO)}$_4$] (**2**).

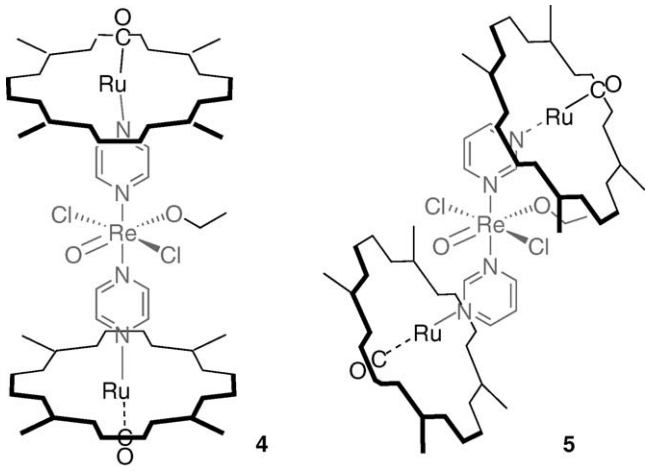

Fig. 11. Schematic representation of the Re(V) linear and tilted bisporphyrin sandwich adducts [{*trans,trans,trans*-ReO(OEt)Cl_2}(μ-pyz)$_2${Ru(TPP)(CO)}$_2$] (**4**) and [{*trans,trans,trans*-ReO(OEt)Cl_2}(μ-pym)$_2${Ru(TPP)(CO)}$_2$] (**5**), respectively (phenyl groups omitted for clarity).

ReO(OEt)Cl_2}(μ-pyz)$_2${Ru(TPP)(CO)}$_2$] (**4**), and the corresponding tilted compound [{*trans,trans,trans*-ReO(OEt)Cl_2}(μ-pym)$_2${Ru(TPP)(CO)}$_2$] (**5**) (Fig. 11) [43].

More recently, we used the bis-pyridyl perylene-bisimide chromophore (PBI) as linear bridging ligand and prepared the corresponding adduct [{Ru(TPP)(CO)}$_2$(μ-PBI)] (**6**), in which two ruthenium porphyrins are axially bound to a central PBI chromophore (Fig. 12) [44].

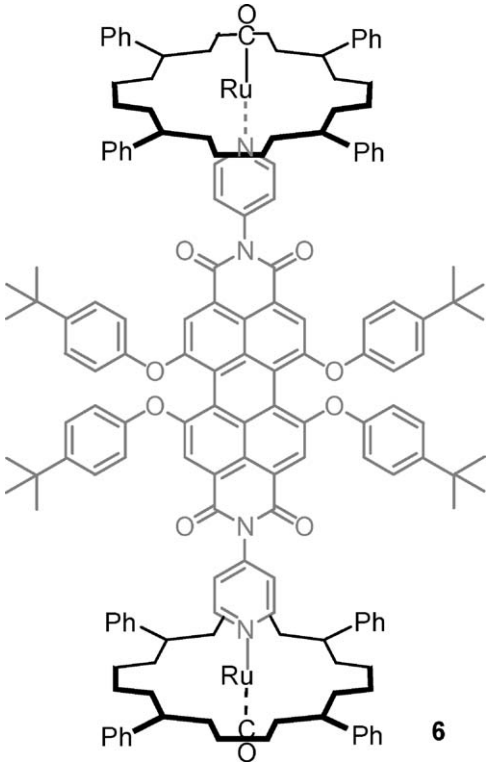

Fig. 12. Schematic drawing of the bisporphyrin/perylene-bisimide assembly [{Ru(TPP)(CO)}$_2$(μ-PBI)] (**6**).

3.2. Ruthenium-mediated discrete assemblies of porphyrins

Within this synthetic approach we mainly exploited the coordination ability of two Ru(II) complexes, *trans*-[$RuCl_2$(dmso-S)$_4$] (**7**) and *trans,cis,cis*-[$RuCl_2$(dmso-O)$_2$(CO)$_2$] (**8**), that behave as neutral *cis* bis-acceptor fragments upon selective replacement, under mild conditions, of two adjacent dmso ligands with heterocyclic N-donor ligands (L) [45].

Thus, treatment of **7** or **8** with a slight excess of 4′MPyP (chloroform, room temperature), yielded the corresponding disubstituted complexes *trans,cis,cis*-[$RuCl_2$(dmso-S)$_2$(4′MPyP)$_2$] (**9**) and *trans,cis,cis*-[$RuCl_2$(CO)$_2$(4′MPyP)$_2$] (**10**), respectively, in which the two adjacent porphyrins are in free rotation about the Ru–N bonds (Fig. 13) [42b,46]. The newly formed Ru–N(pyridyl) bonds on the *trans,cis,cis*-$RuCl_2(X)_2$ fragment (X = dmso-S, CO) are both stable and inert and, as a consequence, the corresponding adducts are very robust.

Similarly, we found that the reaction of the *cis* coordinating ruthenium precursors **7** and **8** with the *angular* porphyrin building block 4′-*cis*DPyP, leads to different products depending on the ligand-to-metal ratios employed: either metallacycles (1:1 ratio) (Scheme 1) or bispophyrin complexes (4:1 ratio) (see below, Fig. 17).

This experimental observation implies that the formation of such products occurs under kinetic control, as it might have been anticipated considering the relatively inert nature of the Ru(II)–N(py) bond. Thus, treatment of the Ru precursors with a stoichiometric amount of 4′-*cis*DPyP led to the formation of the neutral 2 + 2 metallacycles of porphyrins of formula [*trans,cis,cis*-$RuCl_2(X)_2$(4′-*cis*DPyP)]$_2$ (X = dmso-S, **11**; X = CO, **12**) (Scheme 1) [42b,46b,47].

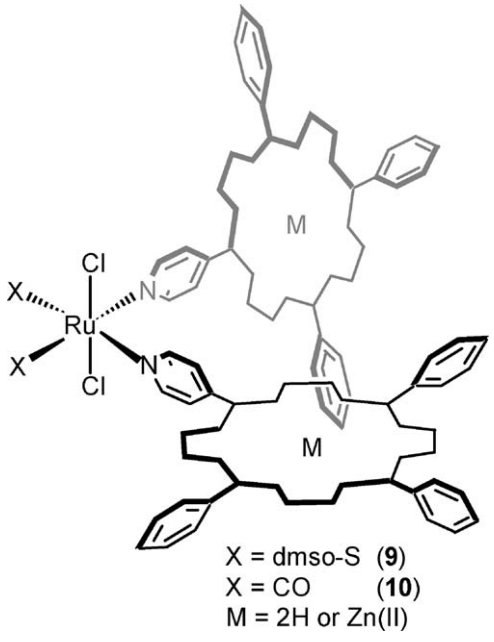

Fig. 13. Schematic drawing of *trans,cis,cis*-[$RuCl_2$(dmso-S)$_2$(4′MPyP)$_2$] (**9**) and *trans,cis,cis*-[$RuCl_2$(CO)$_2$(4′MPyP)$_2$] (**10**), as free-base or zincated derivatives.

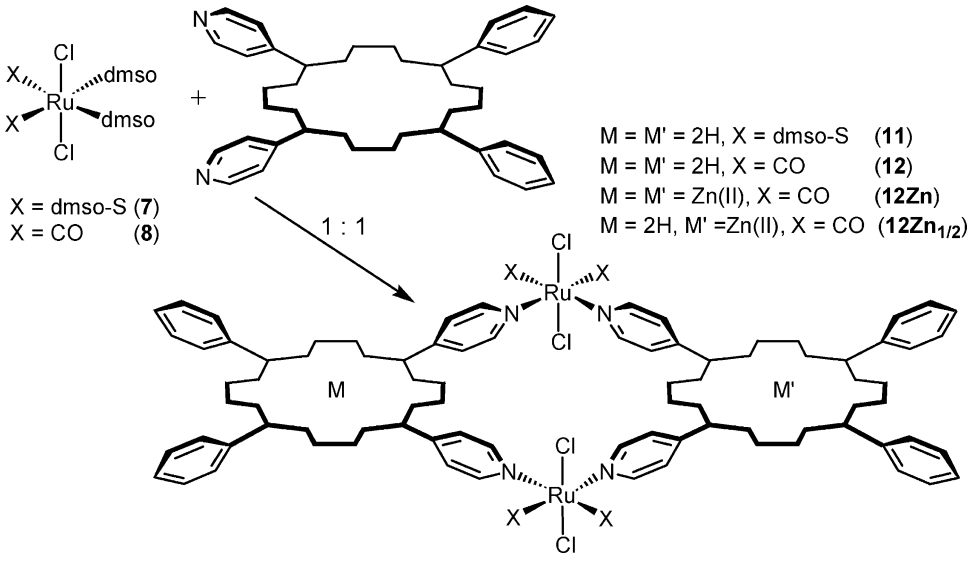

Scheme 1.

These products were purified by column chromatography and fully characterized spectroscopically and by FAB mass spectrometry.

As for the side-to-face assemblies described above, ^{1}H NMR spectroscopy proved particularly useful for characterizing the new Ru–4′PyP compounds. Coordination to ruthenium affects mainly the resonances of the pyridyl ring(s) of 4′PyPs, causing downfield shifts ($\Delta\delta$ H2,6 from 0.3 to 0.9 ppm, $\Delta\delta$ H3,5 from 0.03 to 0.18 ppm, see Fig. 7 for numbering scheme). The dmso-S signals, when present, gave information about the coordination environment of the Ru centers and the symmetry of the assembly. Further evidence for the assignment of the product geometry were obtained from IR and ^{13}C{^{1}H} NMR spectroscopic data concerning the chloride, dmso, and carbonyl ligands.

The ^{1}H NMR spectra of **11** and **12** unambiguously established the metallacyclic nature and high symmetry of these species. A recent X-ray structural determination performed on the zincated derivative of **12**, **12Zn** (see also Section 3.3), showed that in the solid state the metallacycle (C_2 symmetry, with the two-fold axis passing through the Ru atoms) is flat, with an almost perfect coplanar arrangement of the two porphyrins. The Ru···Ru and the Zn···Zn distances are 14.009(3) and 14.028(3) Å, respectively (Fig. 14) [7i].

The reaction of precursor **8** with an equimolar amount of 3′-*cis*DPyP, rather than 4′-*cis*DPyP, yielded the corresponding neutral 2 + 2 metallacycle [*trans,cis,cis*-$RuCl_2(CO)_2$(3′-*cis*DPyP)]$_2$ (**13**) (Fig. 15) [7i].

NMR spectroscopy provided unambiguous evidence that only one highly symmetrical metallacycle, in which the two chromophores are held in a *slipped cofacial* arrangement by the external Ru(II) fragments, exists in solution. We had no evidence of the formation of other possible conformers of **13**, which might derive from different orientations of the 3′N(py) rings with respect to the porphyrin plane. The unprecedented staggered geometry of **13**, and of the similar fully zincated derivative [*trans,cis,cis*-$RuCl_2(CO)_2$(Zn·3′-*cis*DPyP)]$_2$ (**13Zn**),

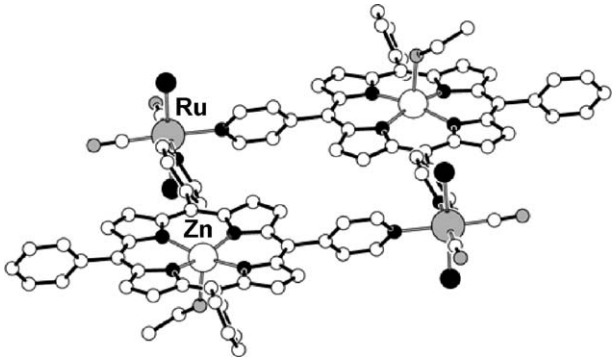

Fig. 14. Front-view of the solid state structure of [*trans,cis,cis*-$RuCl_2(CO)_2$(Zn·4′-*cis*DPyP)(EtOH)]$_2$ (**12Zn**) (adapted from Ref. [7i]).

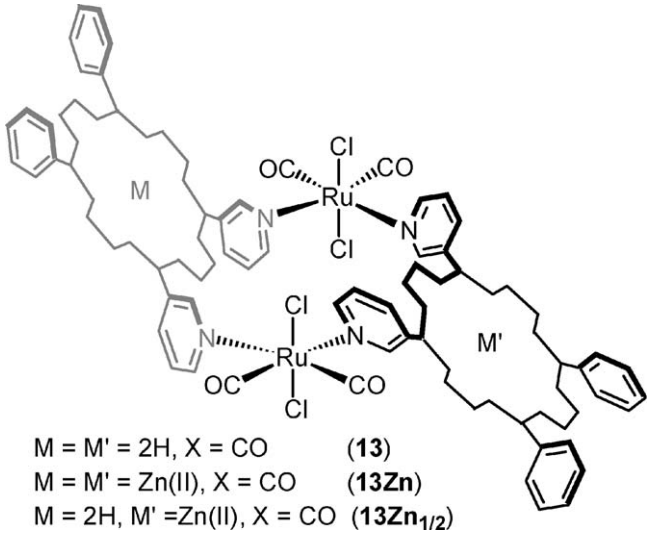

Fig. 15. Schematic representation of the neutral porphyrin metallacycle [*trans,cis,cis*-$RuCl_2(CO)_2$(3′-*cis*DPyP)]$_2$ (**13**), and of its fully and semi-zincated analogues (**13Zn**, **13Zn**$_{1/2}$).

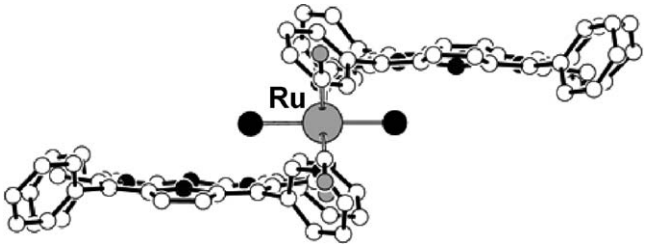

Fig. 16. Side-view (along Ru···Ru) of the molecular structure of [*trans,cis,cis*-$RuCl_2(CO)_2$(3′-*cis*DPyP)]$_2$ (**13**) (adapted from Ref. [7i]).

were confirmed in the solid state by X-ray structural investigations (Fig. 16).

The geometry of **13**, with an interplanar distance between the two porphyrins of 4.18 Å and a lateral offset (center-to-center distance) of 9.819 Å, closely resembles those found for the bacteriophylls of the special pair and of the antenna system (B850) of photosynthetic bacteria. Thus, as anticipated, the change in the position of the N atom in the peripheral pyridyl rings of *cis*DPyP from 4′ to 3′ led indeed, upon coordination to the same *cis* bifunctional ruthenium fragment [*trans,cis*-$RuCl_2(CO)_2$], to porphyrin cyclic assemblies with equal nuclearity, but very different geometries: from a flat two-dimensional one (**12**) to a staggered three-dimensional structure with a rigid spatial arrangement of the two chromophores (**13**).

Conversely, treatment of **7** or **8** with excess 4′-*cis*DPyP under mild conditions led, after chromatographic purification, to the isolation of the corresponding bisporphyrin mononuclear compounds *trans,cis,cis*-[$RuCl_2(X)_2$(4′-*cis*DPyP)$_2$] (Fig. 17, X = dmso-S, **14**; X = CO, **15**). The nature and geometry of the products were established by ^{1}H and ^{13}C NMR spectroscopy [7g,42b,46b].

Compounds **14** and **15** have one residual unbound 4′N(py) ring on each of the two *cis* coordinated 4′-*cis*DPyP units, and are therefore metal-containing ligands. We demonstrated that they are capable of chelating suitable *cis* bis-acceptor

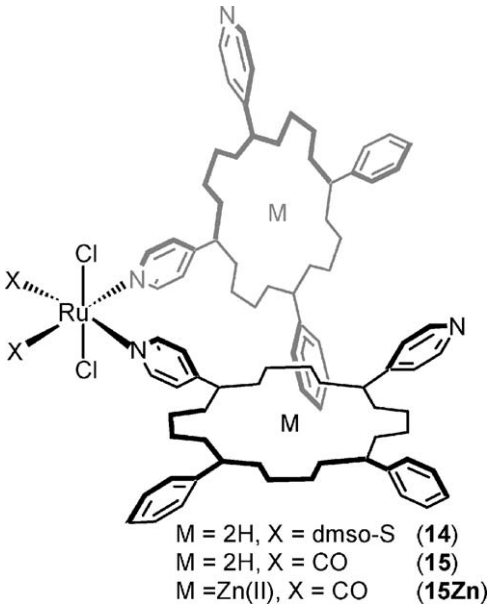

Fig. 17. Schematic drawing of the metal-containing ligands *trans,cis, cis*-[$RuCl_2$(dmso-S)$_2$(4′-*cis*DPyP)$_2$] (**14**), *trans,cis,cis*-[$RuCl_2(CO)_2$(4′-*cis* DPyP)$_2$] (**15**) and its zincated derivative *trans,cis,cis*-[$RuCl_2(CO)_2$(Zn·4′-*cis*DPyP)$_2$] (**15Zn**).

metal fragments. Indeed, ^{1}H NMR spectroscopy established that titration of [Pd(dppp)$(OTf)_2$] into chloroform solutions of either **14** or **15** leads readily to the quantitative formation of the corresponding hetero-bimetallic 2 + 2 metallacycle of porphyrins [Pd(dppp) {*trans,cis,cis*-$RuCl_2(X)_2$(4′-*cis*DPyP)$_2$}] $(OTf)_2$ (Scheme 2, X = dmso-S, **16**; X = CO, **17**), featuring one neutral octahedral Ru(II) and one dicationic square-planar Pd(II) fragment at opposite corners. Product selectivity was not affected by accidental excess of [Pd(dppp)$(OTf)_2$] and no evidence of homo-metallic metallacycles was found.

According to the X-ray structure, the metric parameters of **17** (metal-to-porphyrin center distances of about 9.83 Å, Pd···Ru

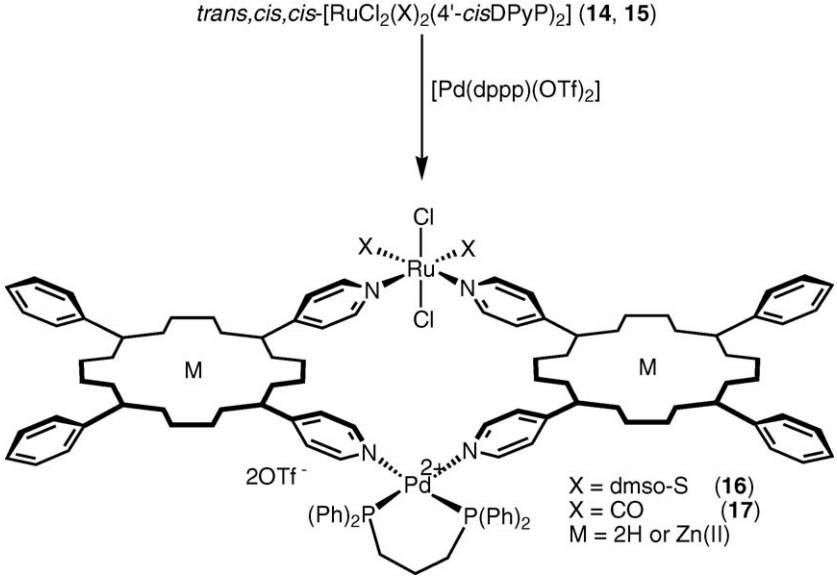

Scheme 2.

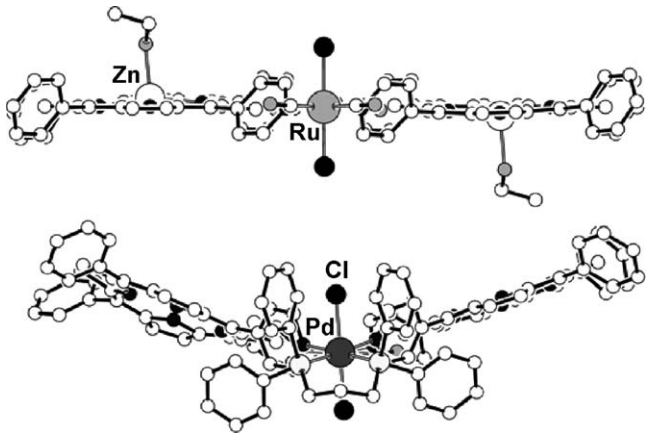

Fig. 18. Side-views of [*trans,cis,cis*-$RuCl_2(CO)_2$(Zn·4′-*cis*DPyP)(EtOH)]$_2$ (**12Zn**) (along Ru···Ru, top, adapted from Ref. [7i]) and of [Pd(dppp){*trans,cis,cis*-$RuCl_2(CO)_2$(4′-*cis*DPyP)$_2$}]$^{2+}$ (**17**) (along Pd···Ru, bottom, adapted from Ref. [7g]).

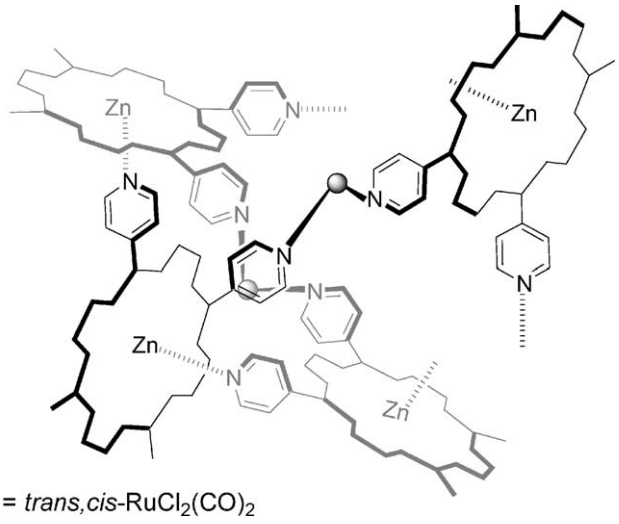

Fig. 19. Schematic representation of possible intermolecular interactions in *trans,cis,cis*-[$RuCl_2(CO)_2$(Zn·4′-*cis*DPyP)$_2$] (phenyl groups omitted for clarity).

diagonal distance of ca. 14.0 Å) are very similar to those found in the corresponding homo-metallic ruthenium metallacycle **12Zn** (see above). However, while in the solid state **12Zn** is almost perfectly flat, **17** exhibits a butterfly conformation with porphyrins least-squares planes that form a dihedral angle of ca. 138°, approximating a C_s symmetry (Fig. 18), similar to what was found by Stang and co-workers in the corresponding "all-palladium" metallacycle [Pd(dppp)(4′-*cis*DPyP)]$_2$(OTf)$_4$ [7h]. Optimization of the stacking interactions between the phenyl rings of the diphosphine bridge and the pyridyl rings of the porphyrins is very likely the driving force leading to this distortion in the solid state.

When the two porphyrins of **15** are zincated, the corresponding *trans,cis,cis*-[$RuCl_2(CO)_2$(Zn·4′-*cis*DPyP)$_2$] complex (**15Zn**) (Fig. 15) features two *donor* (the uncoordinated 4′N(py) atoms) and two *acceptor* (the Zn atoms) sites, whose relative orientation depends on the torsion angles about the Ru–N bonds. It can therefore be expected that these reactive sites interact with each other to give discrete and/or polymeric self-assembled species (Fig. 19) [46b,48].

^{1}H NMR spectroscopy provided unambiguous evidence that **15Zn** self-assembles in $CDCl_3$ solution through the establishment of 4′N(py)–Zn interactions to yield selectively a single, highly symmetrical, discrete species in which all donor and all acceptor sites are involved.

Single crystal X-ray analysis established that this product is a dinuclear species, [*trans,cis,cis*-$RuCl_2(CO)_2$(Zn·4′-*cis*DPyP)$_2$]$_2$ (**18**), that features four porphyrins and six metal atoms (two Ru and four Zn), in which the four 4′N(py) sites and the four Zn sites are mutually saturated (Fig. 20). The NMR data of **18** are consistent with the structure found in the solid state, indicating that in solution the same assembly is maintained. The self-assembled structure is very stable: it runs intact through a column of silica gel and no evidence of dissociation was found in the ^{1}H NMR spectra ($CDCl_3$) of **18** diluted to the limit of detection (ca. 3×10^{-5} M). The high stability of the dinuclear species suggests that the four 4′N(py)–Zn interactions occur with a good degree of cooperativity.

In conclusion, *trans,cis,cis*-[$RuCl_2(CO)_2$(Zn·4′-*cis*DPyP)$_2$] is an unprecedented example of self-complementary metalloporphyrin building block that selectively recognizes itself by two point self-coordination yielding a very stable and symmetrical dimeric species, **18**. While in the literature there are several examples of one-point self-coordination of metalloporphyrins [49], two-point self-coordination is much rarer [50] and no other examples of structurally characterized products have been described.

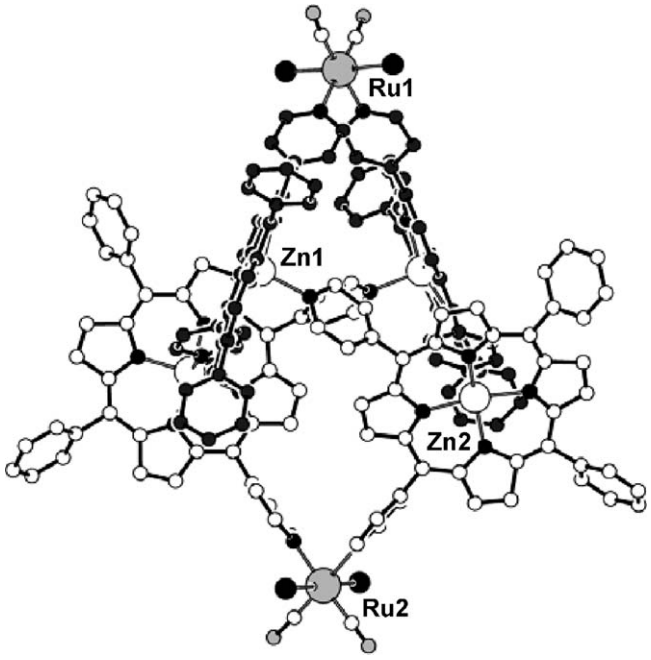

Fig. 20. Perspective view of the solid-state molecular structure of [*trans,cis,cis*-$RuCl_2(CO)_2$(Zn·4′-*cis*DPyP)$_2$]$_2$ (**18**), for clarity the two *trans,cis,cis*-[$RuCl_2(CO)_2$(Zn·4′-*cis*DPyP)$_2$] units have different shades (adapted from Ref. [48]).

3.3. Metal-mediated assemblies of higher order

Treatment of the metallacycles **12** or **13** with excess zinc acetate in chloroform/methanol mixtures led to the isolation of the corresponding fully zincated adduct **12Zn** or **13Zn**, respectively. Similarly, the reaction of **12** or **13** with half equivalent of $Zn(CH_3COO)_2$ afforded in pure form, after chromatographic work-up, the corresponding semi-zincated metallacycles $\mathbf{12Zn}_{1/2}$ and $\mathbf{13Zn}_{1/2}$, in which only one of the two chromophores has an inner zinc atom (see below).

Metallacycle **12Zn**, which is kinetically stable owing to the inertness of the Ru–N(pyridyl) bonds, is a rigid bidimensional molecule with two axial *acceptor* sites, the Zn ions. Thus it can be exploited as a rigid square panel with two central junctions for the construction of more elaborate supramolecular adducts upon treatment with appropriate polytopic N-donor ligands that will bind axially to the Zn atoms. In this approach, a porphyrin supramolecular species becomes in turn, after metallation, a convenient building block for further metal-mediated self-assembly processes.

We found by ^{1}H NMR spectroscopy that titration of **12Zn** with one equivalent of a linear ditopic N-donor ligand leads selectively to the quantitative assembling of sandwich-like 2:2 supramolecular adducts of formula $[(\mathbf{12Zn})_2(\mu\text{-L})_2]$ (L = 4,4′-bipy, **19**; L = 4′-*trans*DPyP, **20**; L = 4′-*trans*DPyP-npm, **21**), consisting of two parallel metallacycles connected *face-to-face* by two bridging ligands which are axially bound to the zinc-porphyrins (Fig. 21) [42b,46b,47].

Compounds **20** and **21**, which feature six porphyrins each, might be better defined as multiporphyrin molecular boxes. Compound **20** was also characterized in the solid state by single-crystal X-ray analysis (Fig. 22). The distance between the two opposite metallacycles, which are slightly warped, is ca. 19.5 Å. The two bridging 4′-*trans*DPyP ligands are cofacial and slightly bowed inward, at a distance of ca. 11.4 Å. The apical 4′N(py) rings bound to the Zn ions are approximately perpendicular to the porphyrin basal planes. The $CDCl_3$ NMR spectrum of **20** is perfectly consistent with the solid state structure, suggesting

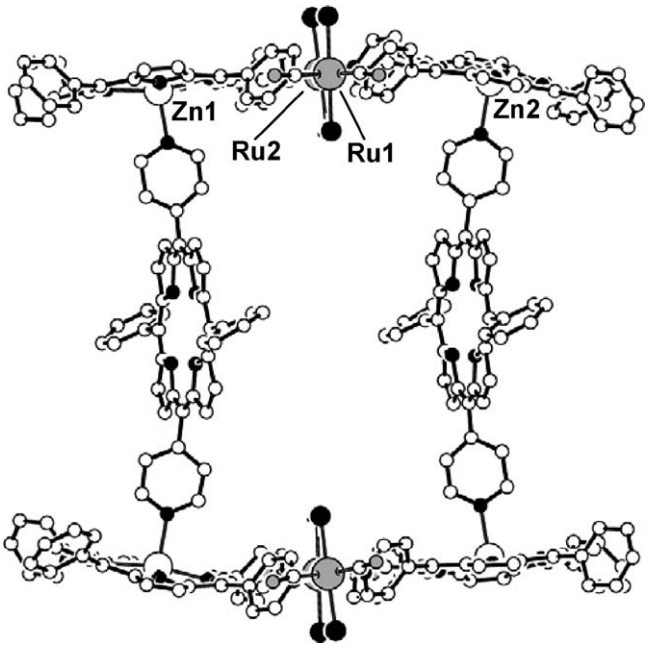

Fig. 22. X-ray structure of the multiporphyrin molecular box $[(\mathbf{12Zn})_2(\mu\text{-}4'\text{-}trans\text{DPyP})_2]$ (**20**) (adapted from Ref. [47]).

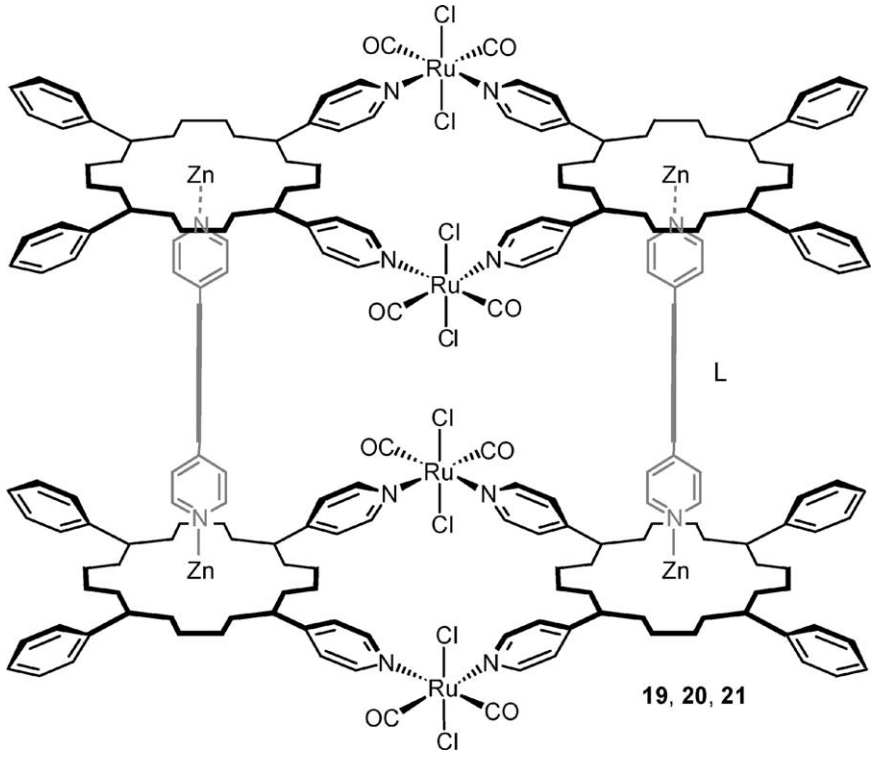

Fig. 21. Schematic drawing of the porphyrin molecular sandwiches **19**–**21** (L = 4,4′-bipy, **19**; L = 4′-*trans*DPyP, **20**; L = 4′-*trans*DPyP-npm, **21**).

that the same geometry, including the cofacial orientation of the two bridging pyridylporphyrins, as an average, is maintained in solution. Even though systems featuring two cofacial porphyrins connected to one another by flexible or rigid organic bridges are well known [51], systems in which the two porphyrins are not covalently linked are rather uncommon.

Formation constants higher than $10^{18}\,M^{-3}$ were estimated in chloroform for compounds **19**–**21** and the ^1H NMR spectra of $CDCl_3$ solutions, diluted to the limit of detection, showed the resonances of the intact assemblies exclusively. The high stability of the adducts was attributed to entropy considerations: owing to the rigidity of the fragments, formation of the sandwich molecules requires limited conformational changes; in addition, there must be considerable cooperativity in the coordination of the two bridging ligands.

Despite the unambiguous NMR evidence that in solution compound **19** exists as a discrete sandwich molecule, X-ray analysis showed that in the solid state it has a different structure, which consists of an infinite wire of porphyrin metallacycles bridged by 4,4′-bipy ligands axially coordinated alternatively on the two opposite faces of each **12Zn** unit, [(**12Zn**)(μ-4,4′-bipy)]$_\infty$.

4. Photophysical properties

4.1. Photophysics of simple porphyrins

In this section, the photophysical behavior of some prototypal porphyrins is summarized, so as to facilitate the subsequent discussion of the supramolecular systems. We use here as convenient experimental cases 4′MPyP, ZnTPP, and [RuTPP(CO)(py)] (Chart 3) [9a].

These systems can be taken as good examples of the general behavior of free-base porphyrins (Fb), zinc metalloporphyrins (Zn), and ruthenium metalloporphyrins (Ru). Minor quantitative changes in the spectroscopic and photophysical behaviors of these chromophores are only expected to occur as a consequence of chemical modifications such as, e.g., exchange of peripheral phenyl with pyridyl groups or axial coordination of an additional ligand (e.g., pyridine) to the metal in the case of Zn.

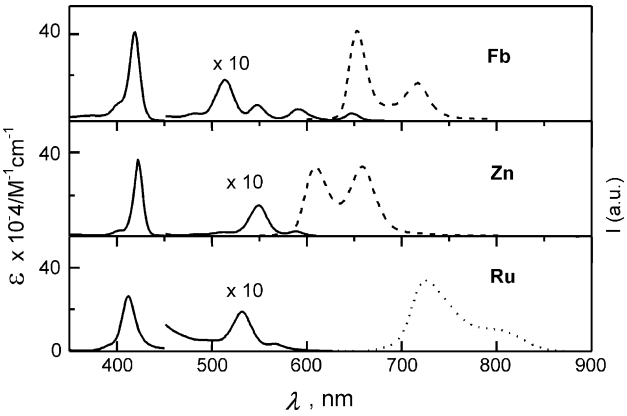

Fig. 23. Absorption and emission (dotted lines) spectra of prototype free-base (Fb), zinc- (Zn), and ruthenium-porphyrin (Ru).

The absorption spectrum of the free-base porphyrins (Fig. 23) involves, besides the intense Soret band, a typical Q-band system made of four distinct vibronic bands. The metalloporphyrins, on the other hand, exhibit a characteristic two-band pattern in the Q-band region. The 0–0 transition is strongly blue shifted upon metallation.

The reasons for the different photophysical behavior of the three types of unit can be discussed in terms of the Jablonski diagrams of Fig. 8. It can be seen that the free-base and zinc-porphyrin have excited singlet states with nanosecond lifetimes, that deactivate via both intersystem crossing to the triplet state (90–95% efficiency) and fluorescent emission (5–10% efficiency). This is the typical behavior of many organic chromophores such as, e.g., aromatic hydrocarbons. By contrast, the behavior of the ruthenium porphyrin is similar to that of typical inorganic chromophores, being dominated by the strong spin–orbit coupling provided by the heavy ruthenium center. Thus, ultrafast intersystem crossing prevents any measurable singlet-state fluorescence. Furthermore, measurable phosphorescence from the triplet state is observed in solution.

Experimentally, the singlet states of free-base and zinc-porphyrins can be conveniently monitored not only by fluorescence spectroscopy but also by picosecond transient absorption

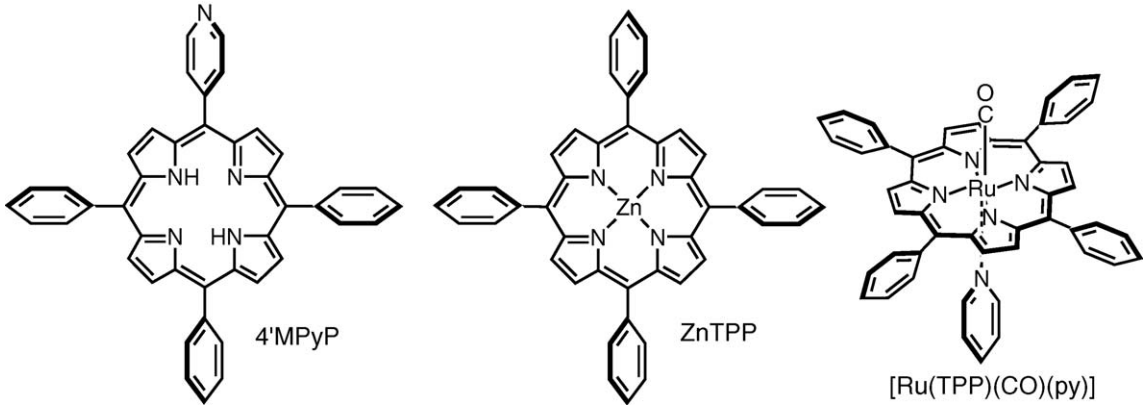

Chart 3.

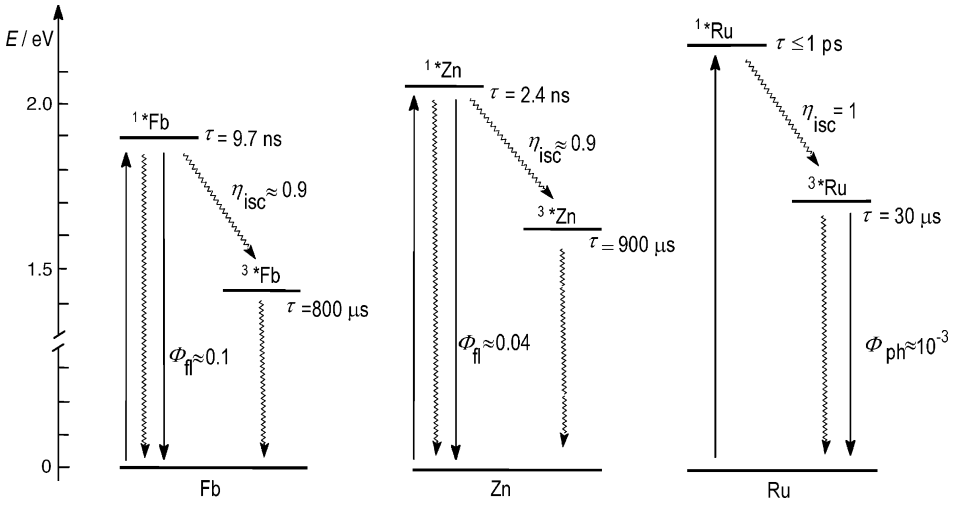

Fig. 24. Energy level diagrams and photophysical mechanisms of prototype free-base (Fb), zinc- (Zn), and ruthenium-porphyrin (Ru).

(Fig. 25). By comparison with the absorption/emission spectra of Fig. 23, it can be seen that the transient spectra consist of a broad featureless positive absorption throughout the visible region, with superimposed bleachings of the ground-state Q-bands and additional apparent bleachings corresponding to stimulated fluorescent emission. As such, the picosecond transient spectra provide good fingerprints for the excited states, particularly useful for diagnostic purposes in supramolecular systems containing various types of chromophores (see, e.g., Sections 4.3 and 4.5).

The triplet states of free-base, zinc-, and ruthenium-porphyrins can be conveniently monitored in nanosecond laser flash photolysis (Fig. 26). The triplet transient spectra exhibit significant differences between the free-base and the metalloporphyrins (Fig. 26) that can be used for diagnostic purposes in multichromophore supramolecular systems (see, e.g., Section 4.4).

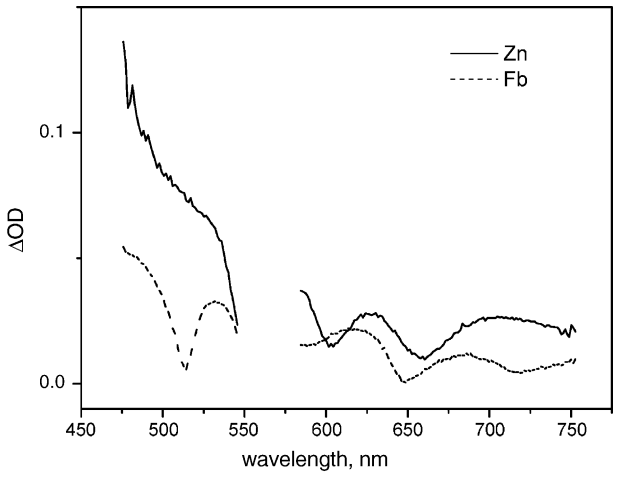

Fig. 25. Transient absorption spectra obtained for free-base and zinc-porphyrin in ultrafast spectroscopy (excitation at 560 nm). Time delay after excitation pulse, 1 ps. Appreciably constant in the 1–1000 ps time range.

4.2. Adducts between pyridylporphyrins and Ru(II) complexes

Adducts **22**–**25**, **9**, **11**, involving different 4′PyPs and octahedral Ru(II) fragments with different ancillary ligands and stereochemistry (*cis,cis*-$RuCl_2(CO)(dmso\text{-}S)_2$ and *trans,cis*-$RuCl_2(dmso\text{-}S)_2$), have been studied (Chart 4) [9d,52]. In these adducts, the Ru(II) fragments are virtually non-absorbing in the visible, so that selective excitation of the pyridylporphyrin is easily achieved. In all the adducts the pyridylporphyrin emit-

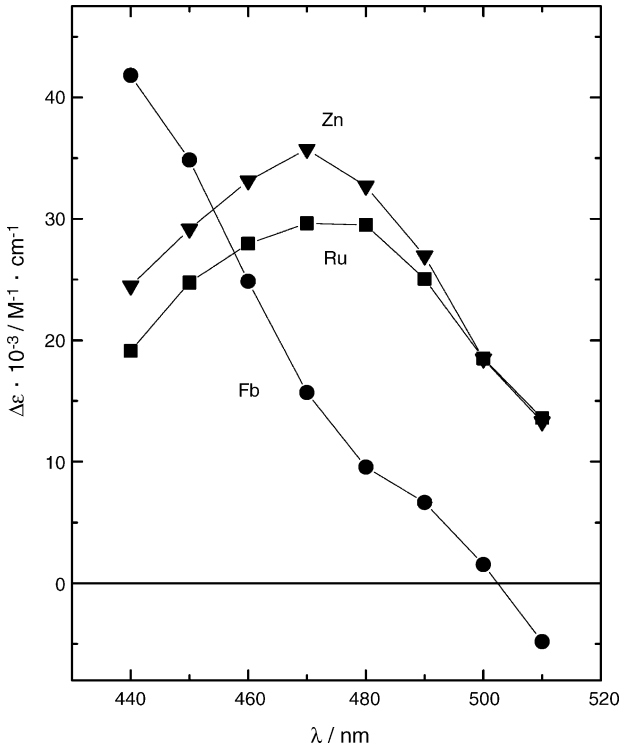

Fig. 26. Triplet difference absorption spectra obtained in the laser flash photolysis of free-base, zinc-, and ruthenium-porphyrin.

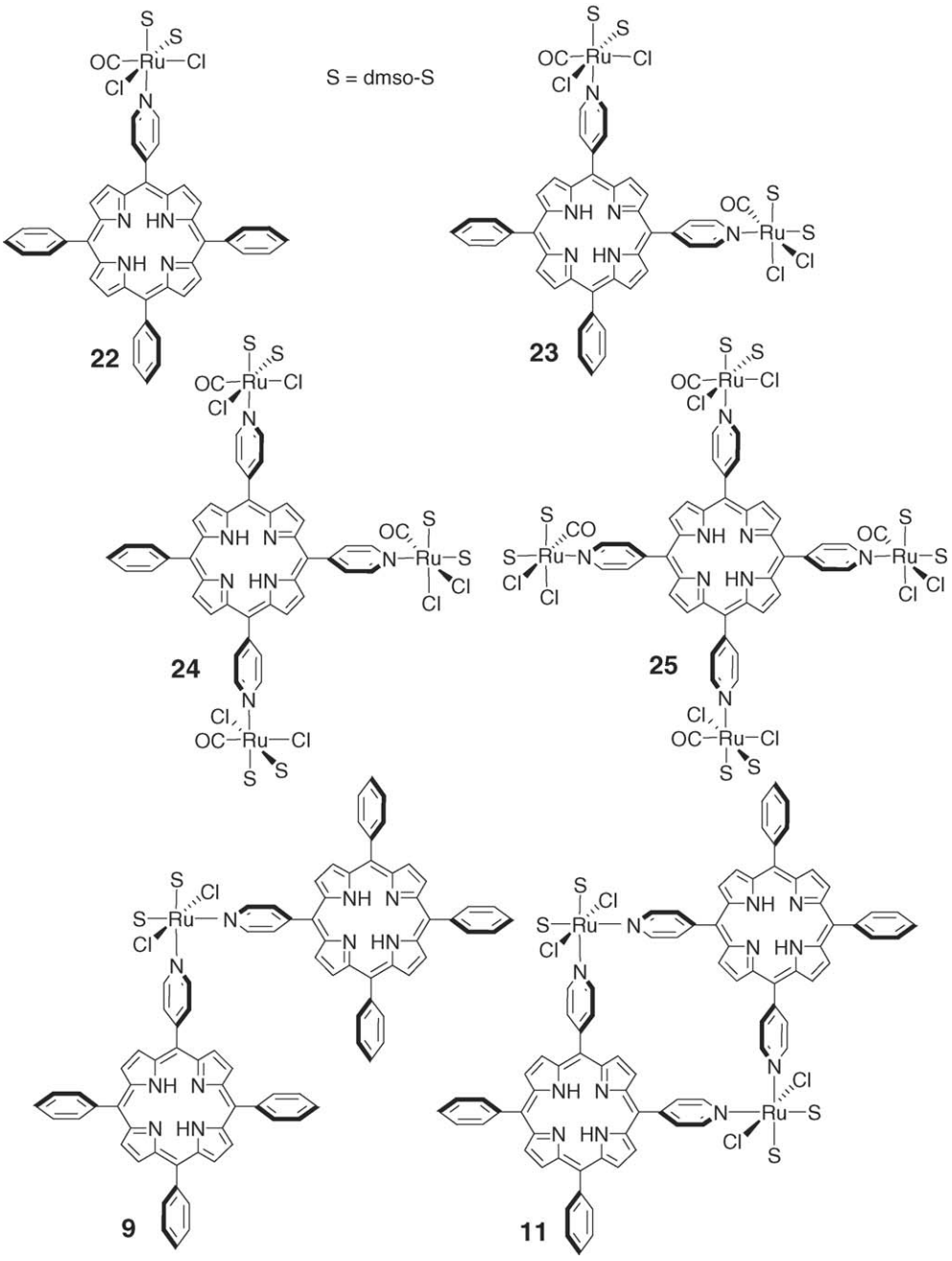

Chart 4.

ting singlet excited state is shorter-lived compared to the parent molecule. The effect, not very large but significant, increases with the number of ruthenium centers attached to each chromophore (Fig. 27). The magnitude of the effect also depends on the nature of the Ru center, being higher for the adducts **9**, **11** than for the series **22**–**25**.

The origin of this lifetime shortening is interesting, since the most obvious quenching mechanisms, singlet energy transfer and photoinduced electron transfer, are prohibited on energetic grounds [52]. A likely explanation of the pyridylporphyrin singlet quenching in the arrays can be identified in the *heavy-atom effect* of the metal. The conventional notion of this effect is that heavy-atom substituents introduce spin–orbit coupling into a molecule, thereby relaxing spin selection rules. In simple molecular systems, the heavy-atom effect quenches the lowest excited singlet state by enhancing intersystem crossing to the triplet. In supramolecular systems of the type we are dealing with here, besides intersystem crossing within the pyridylporphyrin chromophore (k_{ISC}), an additional spin-forbidden channel is available for deactivation of the pyridylporphyrin singlet, i.e., singlet–triplet energy transfer to the attached metal fragment (k_{STEn}) (Fig. 28). In principle, both channels are expected to be sensitive to the heavy-atom effect of ruthenium, although their relative importance is difficult to predict: for k_{ISC} the heavy atom

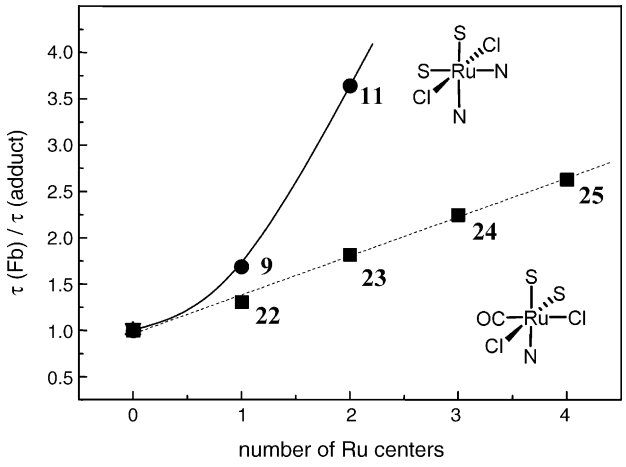

Fig. 27. Porphyrin fluorescence lifetime quenching by coordinated Ru centers in compounds **22**–**25**, **9**, and **11**.

is remote, but the process is an intra-component one; for k_{STEn} the heavy metal center is directly involved, but the process is an inter-component one.

The two types of heavy-atom effects can be experimentally discriminated, as they are expected to induce opposite changes in the population of the pyridylporphyrin triplet in the adduct relative to the free chromophore: slight (if any) increase in the case of enhanced k_{ISC}, decrease in the case of the k_{STEn} pathway. Comparative laser flash photolysis experiments were performed to this purpose [52]. The results seem to indicate different pathways for adducts bearing different Ru centers. In particular, for **25** the porphyrin triplet population is practically the same as for the free-base, suggesting enhanced intersystem crossing (k_{ISC} in Fig. 28) as quenching mechanism. On the other hand, an evident decrease in triplet formation is observed for **9** and **11**, supporting the singlet–triplet energy transfer pathway (k_{STEn} in Fig. 28)

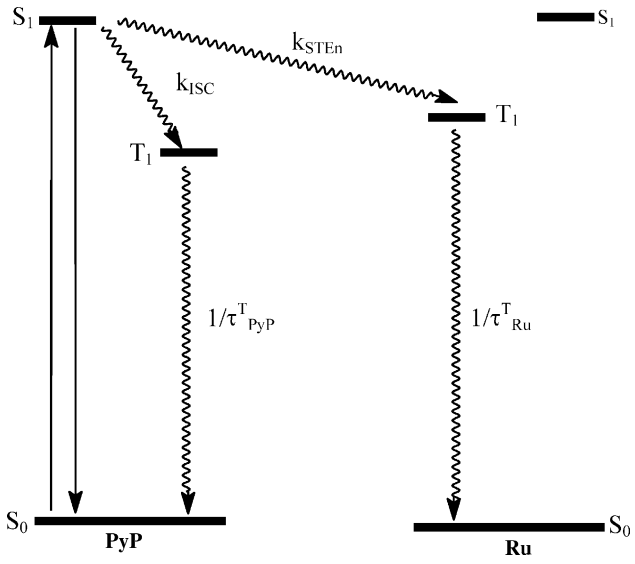

Fig. 28. Possible pathways for pyridylporphyrin fluorescence quenching by heavy-atom perturbation.

as quenching mechanism for these systems. In conclusion, both mechanisms seem to be operative in the adducts studied, the choice being dependent on the type of Ru center. The reasons for the switch in mechanism is not obvious, in the absence of direct information on the triplet energies of the two types of Ru(II) complexes. Ligand field arguments could suggest that the singlet–triplet energy transfer channel may become energetically unavailable for adducts with carbonyl-containing Ru(II) centers [52].

4.3. Metallacycles

The six metallacycles **12**, **12Zn**, **12Zn**$_{1/2}$ and **13**, **13Zn**, **13Zn**$_{1/2}$ contain two *cis* dipyridylporphyrins and two *trans,cis*-$RuCl_2(CO)_2$ corners (see Scheme 1 and Fig. 15). They differ in the pyridyl substituents on the porphyrin, and hence in the overall geometry: **12**, **12Zn**, **12Zn**$_{1/2}$ contain 4′-pyridyl groups and are planar, **13**, **13Zn**, **13Zn**$_{1/2}$ have 3′-pyridyl groups and have a slipped cofacial geometry (see Section 3 for detailed structural information). For each structural type, free-base homo-dimers (**12**, **13**), zinc-porphyrin homo-dimers (**12Zn**, **13Zn**), or free-base/zinc-porphyrin hetero-dimers (**12Zn**$_{1/2}$, **13Zn**$_{1/2}$) are obtained by controlling the degree of zinc insertion. The photophysics of these six metallacycles has been studied in chloroform [7i].

As expected for weakly interacting systems, the absorption spectra of the homonuclear species **12**, **13** and **12Zn**, **13Zn** are very similar to those of the parent free-base and zinc-porphyrin chromophores in the Q-band region (Fig. 23), except for minor spectral shifts. A prominent difference between the planar and the slipped cofacial macrocycles is found in the Soret band region, in which a clear exciton splitting (of ca. 500 cm^{-1}) is present only for the latter compounds (**13** and **13Zn**). This result is as expected on the basis of the relative center-to-center distance in the two types of metallacycles (10.1 Å in the slipped cofacial geometry as compared to 14.1 Å in the planar systems). The photophysics of the homo-dimers is very similar to that of the corresponding monomeric species. In particular, **12** and **13** exhibit the typical fluorescence of the free-base (**12** $\lambda_{max} = 655, 716$ nm, $\tau = 5.7$ ns; **13** $\lambda_{max} = 656, 716$ nm) and **12Zn** and **13Zn** that of Zn-porphyrins (**12Zn** $\lambda_{max} = 608$, 651 nm, $\tau = 1.1$ ns; **13Zn** $\lambda_{max} = 600$, 651 nm). The lifetimes (**12** and **13**, 5.5 ns; **12Zn** and **13Zn**, 1.04 ns) are somewhat shortened (by 30–40%) with respect to the porphyrin components, as a consequence of the heavy-atom effect of the external ruthenium centers (see Section 4.2 for a detailed account of this phenomenon).

The behavior of the hetero-dimers **12Zn**$_{1/2}$ and **13Zn**$_{1/2}$ is more interesting, as in these systems a substantial energy gradient exists between the two chromophores (Fig. 24). The absorption spectra of these semi-zincated species reflect with reasonable approximation the superposition of those of the free-base and Zn-porphyrin components, as shown, e.g., for **13Zn**$_{1/2}$ in Fig. 29. An important consequence is that, besides selective excitation of the free-base porphyrin at $\lambda > 600$ nm, substantial excitation of the zincated porphyrin can be obtained in the hetero-dimers with light of ca. 550 nm.

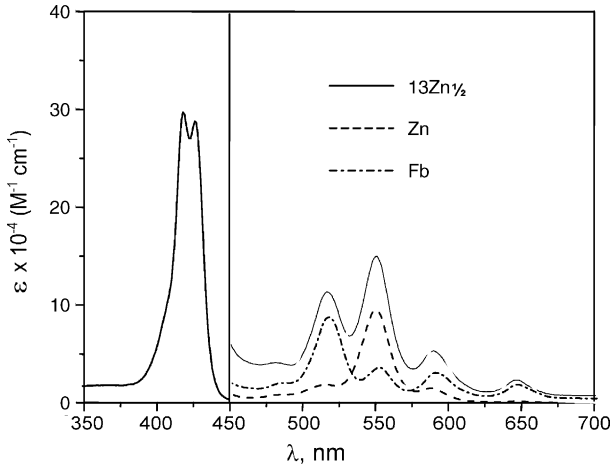

Fig. 29. Comparison between the absorption spectrum of **13Zn**$_{1/2}$ and those of free-base (Fb) and Zn-porphyrin (Zn) monomeric models.

In the semi-zincated species, free-base fluorescence (**12Zn**$_{1/2}$ λ_{max} = 658, 719 nm, τ = 5.0 ns; **13Zn**$_{1/2}$ λ_{max} = 654, 718 nm, τ = 5.3 ns) is always observed, regardless of the excitation wavelength. This demonstrates the occurrence of efficient intramolecular singlet energy transfer from the Zn-porphyrin to the free-base unit. The efficiency of this process can be estimated by an appropriate comparison of the fluorescence intensity observed upon 550 nm excitation (ca. 70% Zn-porphyrin absorption) with that obtained upon 646 nm excitation (100% free-base absorption). The emission intensities obtained for the two excitation wavelengths are identical within experimental error, indicating that for both **12Zn**$_{1/2}$ and **13Zn**$_{1/2}$, the efficiency of singlet energy transfer is $\geq$0.95.

The energy transfer process can be conveniently monitored by ultrafast (femtosecond) spectroscopy, using 555 nm excitation pulses so as to achieve substantial excitation of the Zn-porphyrin chromophore. The spectral changes obtained for the slipped cofacial hetero-dimer **13Zn**$_{1/2}$ are shown in Fig. 30. Consistent with the partitioning of the exciting light, the initial difference

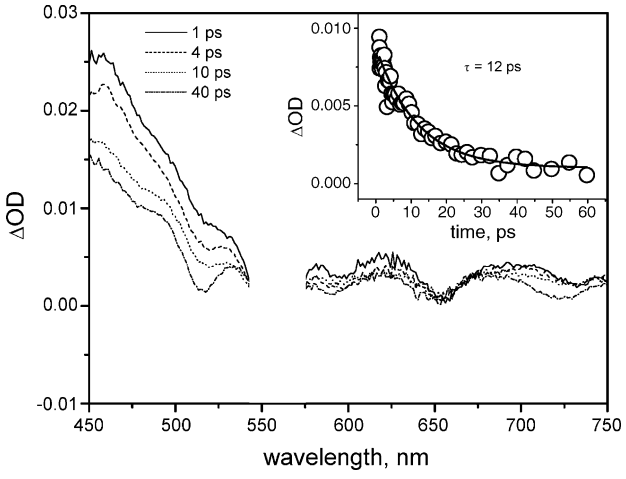

Fig. 30. Transient spectral changes obtained for **13Zn**$_{1/2}$ in $CHCl_3$. Inset: decay kinetics recorded at 515 nm. Excitation wavelength, 555 nm.

spectrum is similar to that of the isolated Zn-porphyrin chromophore (Fig. 25). Very rapidly, however, the transient spectrum undergoes substantial changes, with decreasing absorbance in the short-wavelength region and a characteristic bleaching developing at 515 nm. The final, constant spectrum reached after 40 ps matches very closely that of the free-base porphyrin (Fig. 25). These spectral changes provide clear direct evidence for the occurrence of intramolecular singlet energy transfer in **13Zn**$_{1/2}$ from the Zn-porphyrin to the free-base unit. The time constant of this process is 12 ps, corresponding to a rate constant $k = 8.3 \times 10^{10}\ s^{-1}$. This value is close to (actually slightly higher than) what expected on the basis of Förster theory of dipole–dipole energy transfer (see Section 2.1).

The results of the femtosecond experiments for the planar semi-zincated metallacycle **12Zn**$_{1/2}$ are very similar to those described above for the slipped cofacial analogue with clear evidence for singlet energy transfer from the Zn-porphyrin to the free-base unit. The kinetics give a time constant of 14 ps, again very similar to that obtained for **13Zn**$_{1/2}$. This result is somewhat surprising as, allowing for the different orientational factors, the longer center-to-center distance (14.1 Å in **12Zn**$_{1/2}$ versus 10.1 Å in **13Zn**$_{1/2}$, Fig. 31) would imply a smaller dipole–dipole interaction and substantially slower Förster energy transfer (Eq. (4)). A plausible explanation can be offered considering that singlet energy transfer in these systems may involve, in addition to through-space dipole–dipole interaction, also some through-bond exchange interaction. Since in the ruthenium-bridged porphyrin metallacycles, through-bond interactions are expected to be more effective with 4′- rather than for 3′-pyridyl units (*para* rather than *meta* conjugation), in the planar macrocycle a better exchange coupling could compensate for a weaker dipole–dipole interaction [7i].

4.4. Side-to-face assemblies

As described in Section 3.1, stable and inert side-to-face arrays can be obtained by axial coordination of a pyridylporphyrin ("side" unit) to peripheral ruthenium-porphyrins carrying CO as the sixth ligand ("face" units). Depending on the number of peripheral units, the state of metalation of the pyridylporphyrin, and the binding geometry imposed by the pyridyl groups, a variety of systems of this type is available. The dimeric orthogonal (**26**, **26Zn**) and tilted (**1**, **1Zn**) assemblies are represented schematically in Chart 5.

The orthogonal pentameric arrays **2** and **2Zn** were shown in Fig. 10. The corresponding tilted pentameric species **3**, analogous to **2** but with 3′-pyridyl connecting groups, was also

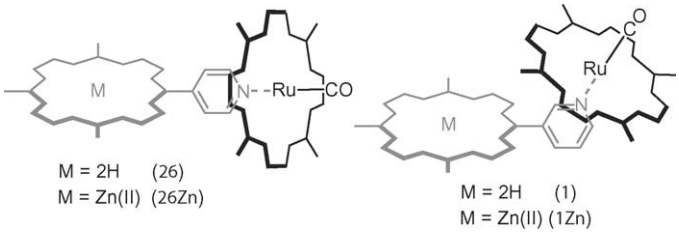

Chart 5.

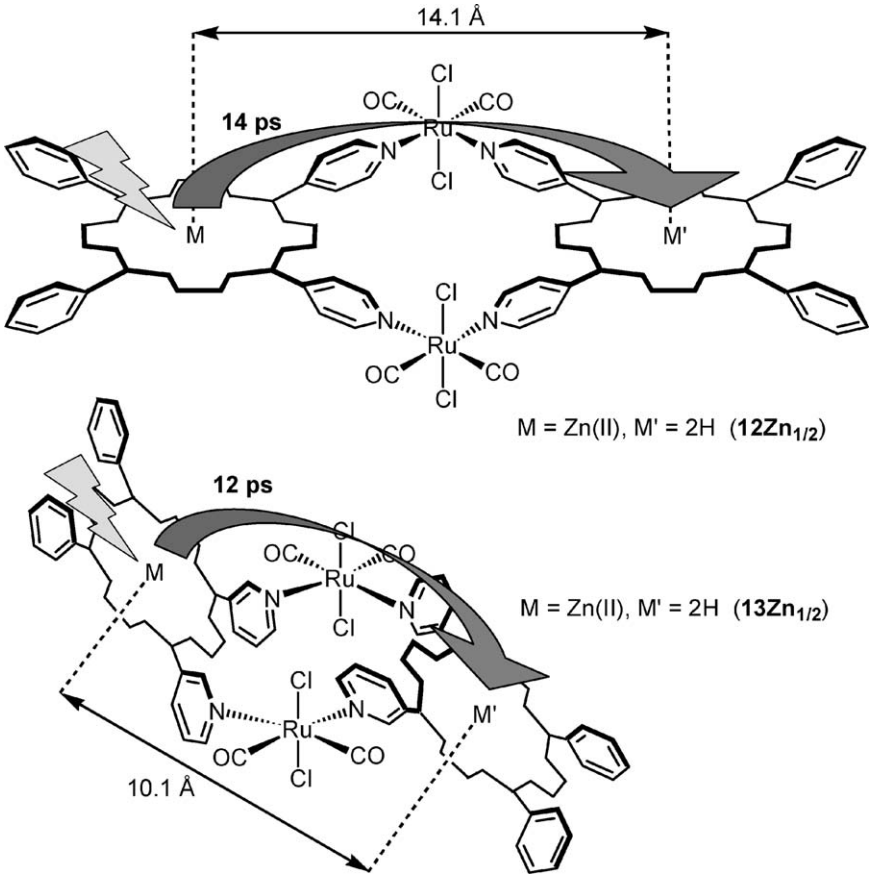

Fig. 31. Center-to-center distances and singlet energy transfer time constants for planar and slipped cofacial hetero-dimers $\mathbf{12Zn}_{1/2}$ and $\mathbf{13Zn}_{1/2}$.

available. The photophysics of all these arrays have been studied [9a] in toluene (where these species are stable in the concentration range $\geq 5 \times 10^{-6}$ M). The results are briefly summarized and discussed in this section.

The side-to face assemblies **26** and **2** contain two types of molecular components, ruthenium-porphyrin units and a free-base porphyrin. The behavior of the monomeric models of these units, Ru and Fb, have been summarized in Section 4.1. As expected for supramolecular species, the absorption spectra of the arrays are always a good superposition of those of the molecular components (Fig. 23). Thus, a general energy level diagram for these arrays can be easily obtained as a combination of those of the Fb and Ru models (Fig. 24). Following selective excitation of the free-base porphyrin at 640 nm, the main observation is that of a significantly shortened fluorescence lifetime. This is the consequence of the heavy-atom effect of the ruthenium center, similarly to that discussed in Section 4.2 for adducts with pyridylporphyrins coordinated to external ruthenium centers (in fact, systems **26** and **2** can be considered similar to adducts **22** and **25** of Section 4.2, by replacing the axially coordinated Ru-porphyrin/s with one or four ruthenium complexes). More interesting is the behavior observed following excitation with 530 nm light, predominantly absorbed by the ruthenium porphyrin chromophore(s). The relevant experimental observations can be summarized as follows: absence of sensitized free-base fluorescence, complete quenching of the Ru porphyrin phosphorescence, prompt 100% formation of free-base triplet in nanosecond laser flash photolysis. These results clearly demonstrate that, after quantitative population of the Ru porphyrin triplet by ultrafast intersystem crossing, the energy is efficiently transferred to the free base unit at the triplet level (Fig. 32). The time constant of this process, measured by ultrafast spectroscopy, is 120 ps for both **26** and **2** [53].

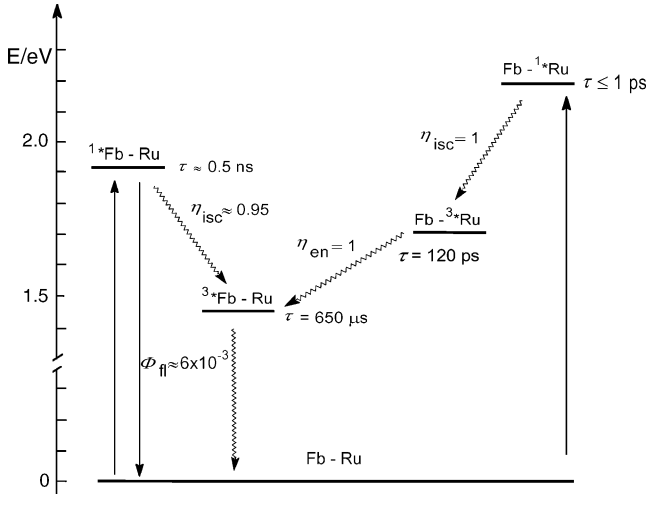

Fig. 32. Photophysical mechanism of pentameric side-to-face array **2**.

For the analogous zinc-containing species, **26Zn** and **2Zn**, a similar qualitative behavior is obtained. The main quantitative differences arise from the fact that the driving force for intercomponent energy transfer is smaller than in the corresponding free-base systems (see the energy levels of the molecular components in Fig. 24). As a consequence, the triplet–triplet energy transfer is now a reversible process. The result is an excited-state equilibrium, in which the Ru-porphyrin and Zn-porphyrin triplets have identical lifetimes [9a].

When the tilted arrays (e.g., **1** and **1Zn**) are compared with the corresponding orthogonal ones (**26** and **26Zn**), the change in connecting structural motif leads to no appreciable qualitative differences in photophysical behavior. The differences are minor even from the quantitative viewpoint, as the triplet energy transfer time constant of **1** is 150 ps (as compared to 120 ps for **26**) [53]. The fact that, despite the smaller center-to-center distance, the rate of **1** is similar to (or even slightly slower than) that of **26** demonstrates the through-bond nature of the exchange interaction responsible for the triplet energy transfer process (Section 2.1).

In conclusion, the side-to-face arrays reviewed in this section behave as very efficient systems for funneling, at the *triplet* level, the light energy absorbed by the peripheral ruthenium porphyrin units to the central free-base or zinc-porphyrin unit (Fig. 33). This behavior can be considered as an example, albeit at the triplet level, of antenna effect. In an interesting extension of this work, efficient energy transfer was observed to occur in a host–guest system formed between the pentameric antenna **2** and a C_{60} molecule [54].

4.5. Structural analogues with perylene bisimides

As discussed in Section 3.1, interesting assemblies can be produced using bis-pyridyl perylene-bisimide (PBI) units as linear bridging ligands. In terms of structural role, PBI can be considered analogous to a ditopic porphyrin ligand such as, e.g., 4′-*trans*DPyP. At difference with the porphyrins, however, perylene bisimides undergo facile electrochemical reduction and are thus more likely to be involved in photoinduced electron transfer processes. Moreover, the high fluorescence yield and the clear spectroscopic signatures of the radical anion form [55,56] make these chromophores ideally suited for photophysical studies.

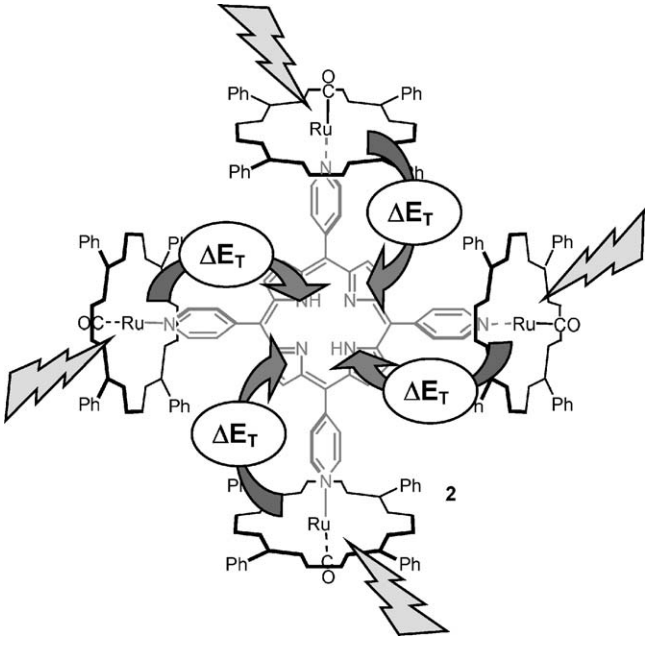

Fig. 33. Schematic representation of the triplet antenna effect in the pentameric side-to-face array **2**.

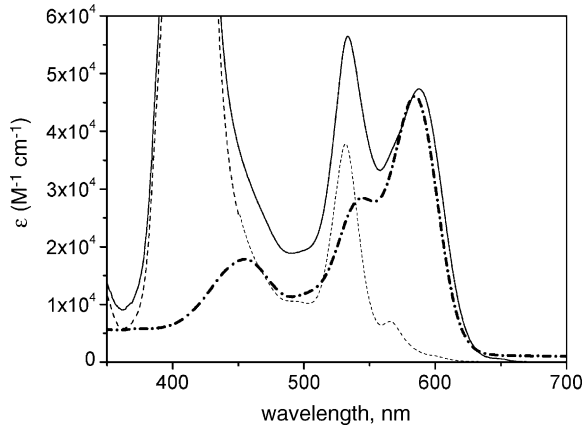

Fig. 34. Absorption spectra of **6** (continuous line), PBI (dash-dot line), and [Ru(TPP)(CO)(py)] (broken line, 2×).

In the bisporphyrin sandwich compound **6** (Fig. 12), two ruthenium porphyrins are axially bound in a side-to-face fashion to a central PBI chromophore. The photophysics have been studied in dichloromethane (where the assembly is stable at concentrations $>2 \times 10^{-5}$ M) [44]. As expected, the absorption spectrum of **6** corresponds very closely to the sum of those of its molecular components (Fig. 34). Experimentally, this implies that selective excitation of the two types of chromophores is feasible (e.g., 100% PBI at 585 nm, 62% Ru(TPP)(CO) at 530 nm). The energy level diagram of **6** (Fig. 35) can be considered as a simple superposition of those of the separated constituents, with the addition of a charge transfer state in which PBI is reduced and the Ru porphyrin is oxidized (energy estimated from electrochemistry). Upon excitation at 585 nm, where the light is 100% absorbed by the PBI component, the strong fluorescence ($\lambda_{max} = 620$ nm) characteristic of the PBI unit is almost completely quenched. The transient spectral changes obtained following 585 nm excitation of **6** (Fig. 36) reveal the mechanism of such quenching. The differential absorption spectrum obtained immediately after the laser pulse corresponds to the singlet state of the PBI unit. In the early timescale ($t < 50$ ps, Fig. 36, top left) the spectral changes are characterized by the rise of the typical absorption band of the PBI radical anion at ca. 780 nm, clearly indicating a reductive photoinduced electron transfer process. The time constant of this process is 5.6 ps (Fig. 36, top right). On a longer timescale ($50 < t < 1000$ ps, Fig. 36, bottom left) the spectroscopic signatures of the intercomponent electron transfer products disappear, with regeneration of a constant baseline of zero differential absorption. This indicates that the charge separation process is followed by charge recombination (time constant 270 ps, Fig. 36, bottom right) to yield quantitatively the ground state of the system (Fig. 35) [44].

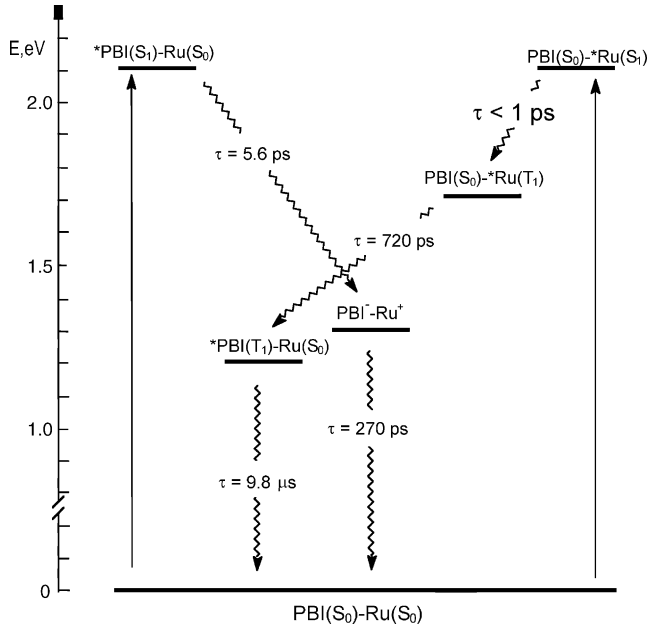

Fig. 35. Photophysical pathways in [{Ru(TPP)(CO)}$_2$(μ-PBI)] (**6**). Red, excitation at 530 nm; blue, excitation at 585 nm.

The ultrafast spectroscopy obtained upon excitation at 530 nm, where the light is absorbed ca. 62% by Ru(TPP)(CO), differs dramatically from that of Fig. 36. The spectral variations now show the disappearance of the Ru-porphyrin triplet state, accompanied by depletion of ground-state and formation of triplet PBI (time constant 270 ps). This demonstrates that, after prompt intersystem crossing within the Ru-porphyrin units, efficient triplet energy transfer to the PBI unit takes place (Fig. 35). The decay of the PBI triplet, as monitored in laser flash photolysis, occurs in a much slower time scale, with a time constant of 9.8 μs [44].

In conclusion, the side-to-face assembly **6** incorporating a perylene bisimide chromophore exhibits complex, interesting photophysics schematically summarized in Fig. 37. It provides a rather striking example of wavelength-dependent behavior, in that a relatively small change in excitation wavelength (from 585 to 530 nm) causes a sharp change in photophysical behavior (from intramolecular electron transfer to triplet energy transfer). The triplet state of the perylene bisimide, inaccessible in the free chromophore due to high fluorescence quantum yields and negligible intersystem crossing efficiency, is efficiently accessed in **6** by means of intramolecular sensitization.

4.6. Higher order assemblies

As discussed in Section 3.3, various multiporphyrin molecular boxes can be obtained that combine both metal-mediated and side-to-face assembling motifs. The chemical structure of the molecular box **20**, resulting from side-to-face self-assembling of two **12Zn** metallacycles and two 4′-*trans*DPyP units, is shown in Fig. 38 (for the X-ray structure, see Fig. 22). The photophysics of this interesting supramolecular system has been studied in chloroform (where the system is stable at concentrations $>7 \times 10^{-5}$ M) [57].

The molecular box **20** contains two types of chromophores, zinc-porphyrin and free-base porphyrin. The behavior of the monomeric models of these units, Zn and Fb, have been summarized in Section 4.1. As expected for supramolecular species, the absorption spectrum of the box is a good superposition of those (Fig. 23) of the molecular components. The energy level diagram for the molecular box, obtained as a combination of

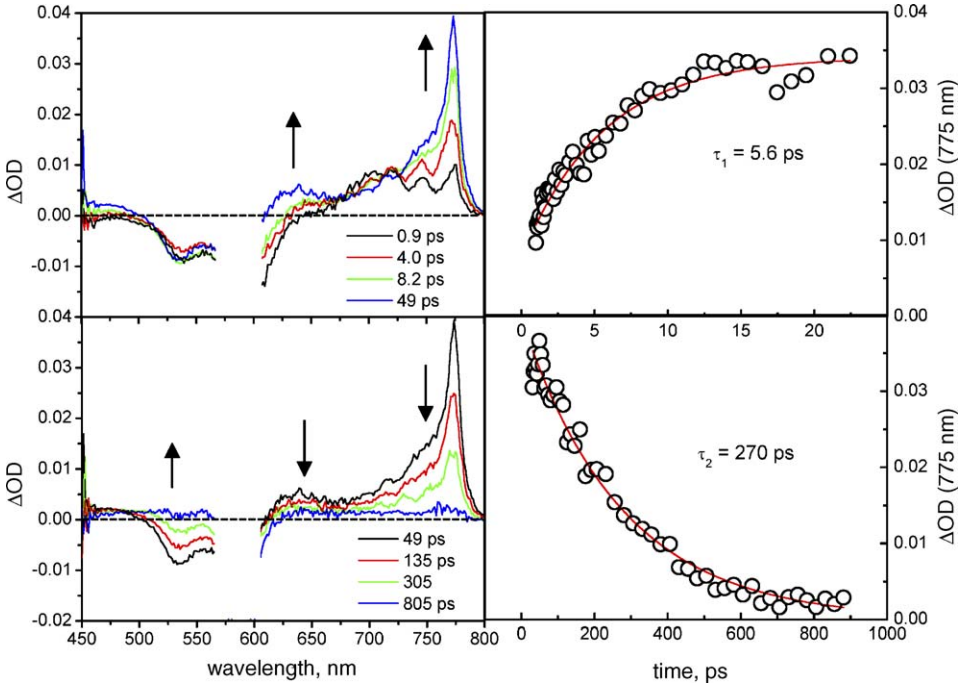

Fig. 36. Transient spectral changes (left) and decay kinetics (right) of **6** in CH_2Cl_2 obtained with ultrafast spectroscopy upon excitation at 585 nm. Top, early time scale (0.9–48 ps); bottom, longer time scale (48–805 ps).

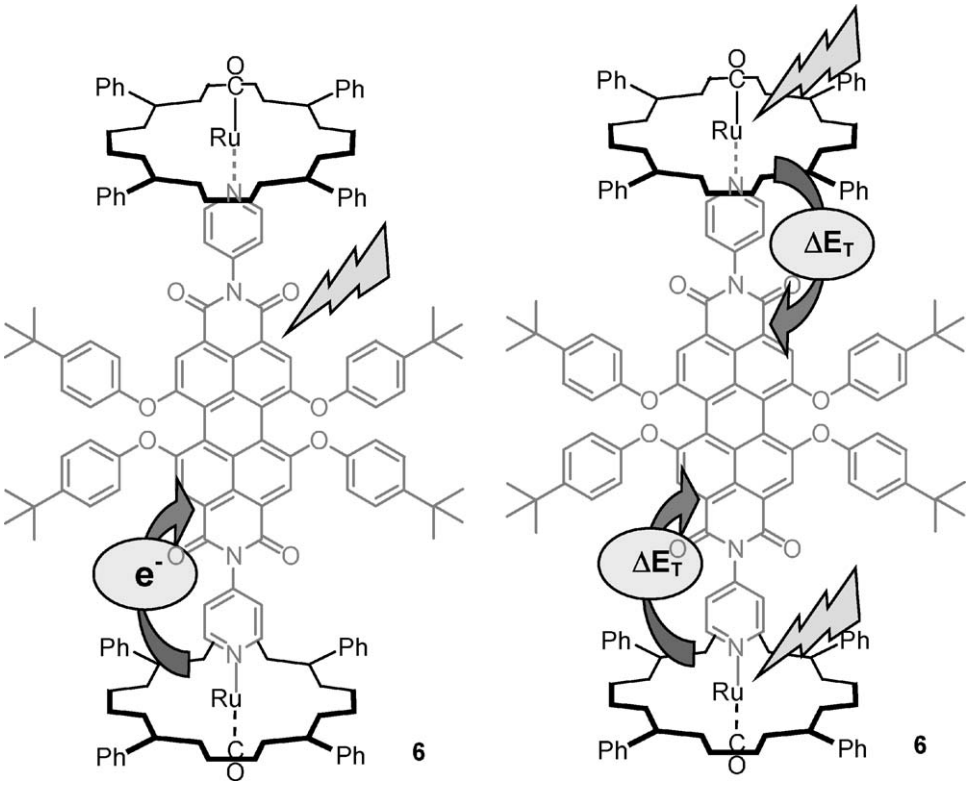

Fig. 37. Schematic representation of the complex, wavelength-dependent electron/energy transfer behaviors of **6**.

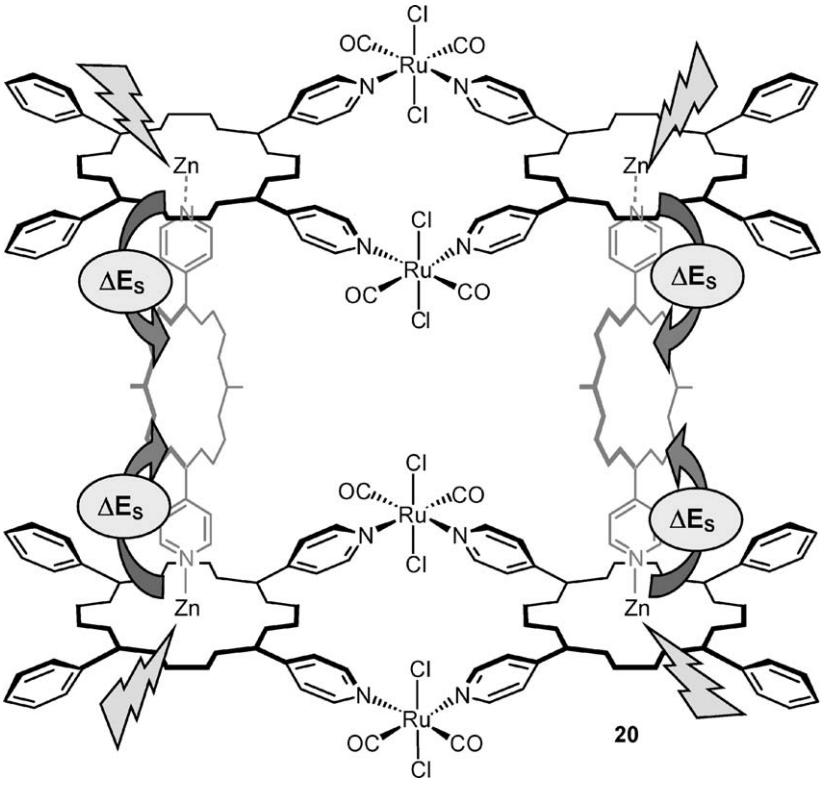

Fig. 38. Schematic representation of the molecular box **20**, phenyl groups of the pillar porphyrins are omitted for clarity, and schematic representation of its antenna effect.

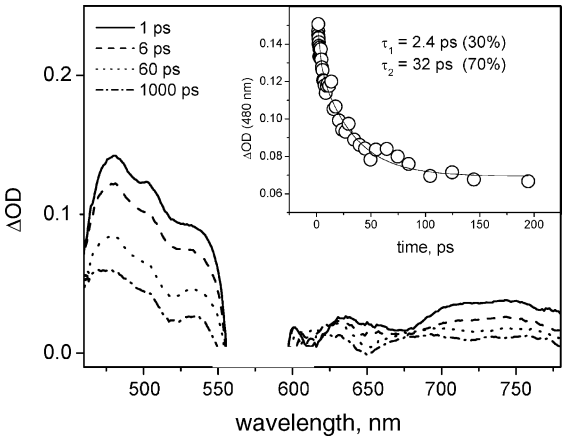

Fig. 39. Transient spectral changes observed in the ultrafast spectroscopy of **20** (excitation at 569 nm).

those (Fig. 24) of the Fb and Zn models, shows a significant driving force for energy transfer from the Zn-porphyrins to the free base units.

Selective excitation of the free-base chromophores in the molecular box can be carried out at 640 nm, yielding the typical fluorescence of this unit. When excitation is carried out at 569 nm, on the other hand, light is predominantly absorbed by the Zn-porphyrin units. Very weak fluorescence is obtained from these units, however, whereas intense free-base fluorescence is again observed. This clearly indicates the occurrence of singlet energy transfer in the molecular box. The energy transfer process can be directly monitored by ultrafast spectroscopy (Fig. 39), where the process is demonstrated by the disappearance of the zinc-porphyrin absorption in the 450–550 nm range and the appearance of the characteristic free-base bleachings (see, for comparison, the spectra of the Zn and Fb models in Fig. 25).

The singlet energy transfer is very fast. The complex kinetics (best fit obtained with time constants of 2.4 and 32 ps) can be attributed to an appreciable degree of conformational freedom in the molecular box. A quantitative estimate of the sensitization efficiency, performed by comparing the intensity of the free-base emission upon free-base or zinc porphyrin excitation, yields a value of 0.5, indicating that some additional fast process competes with energy transfer for deactivation of the zinc-porphyrin singlet excited state. Oxidative electron transfer quenching can be considered as a plausible competing deactivation channel [57].

In conclusion, the molecular box **20** provides a good example of antenna effect, whereby the light energy absorbed by the four Zn-porphyrin units is funneled by means of singlet–singlet energy transfer to the pillar free-base units (Fig. 38). Of particular interest in this regard is the fact that the molecular box has a central cavity that could, in principle, be used to host a variety of species capable of establishing π stacking interactions with the free-base units (e.g., aromatic hydrocarbons, aromatic bisimides, fullerenes). This could open the way towards more complex functional systems.

5. Conclusions and perspectives

The formation of coordination bonds between the peripheral donor sites of pyridylporphyrins and external metal centers has proved to be a very versatile and powerful synthetic approach for the construction of discrete, ordered multiporphyrin assemblies.

When the metal centers belong to metalloporphyrins, side-to-face assemblies of axially ligated porphyrins, either orthogonal (with 4′PyP's) or tilted (with 3′PyP's), are obtained. In the absence of additional cooperative bonding, adducts of sufficient thermodynamic and kinetic stability to allow photophysical investigations are obtained with Ru(CO)-porphyrins, but not with the corresponding Zn-porphyrins.

When the metal centers belong to external coordination compounds, robust and shape-persistent three-dimensional structures with precise size and shape can be efficiently obtained.

Despite the increasing structural complexity and beauty of the metal-mediated assemblies of porphyrins prepared in recent years, the number of multitopic metal fragments used so far is still limited. Thus, we believe that in future the exploitation of a larger variety of metal connectors, in terms of geometries and coordination numbers, will provide even more structurally sophisticated assemblies. For this reason, while we have already exploited the coordination chemistry of octahedral complexes that are precursors of 90° *cis* bis-acceptor neutral fragments, we are currently investigating Ru(II) and Re(I) compounds that might allow coordination of three pyridylporphyrins in a facial geometry.

It is also remarkable how, by changing the position of the ligating N atom of PyP's from 4′ to 3′, we obtained and structurally characterized assemblies with equal nuclearities, but very different geometries: see for example the orthogonal and tilted pentamers $[(4'\text{TPyP})\{\text{Ru(TPP)(CO)}\}_4]$ (**2**) and $[(3'\text{TPyP})\{\text{Ru(TPP)(CO)}\}_4]$ (**3**), respectively, or the flat bidimensional and the staggered tridimensional metallacycles [*trans,cis,cis*-$\text{RuCl}_2(\text{CO})_2$(4′-*cis*DPyP)]$_2$ (**12**) and [*trans,cis,cis*-$\text{RuCl}_2(\text{CO})_2$(3′-*cis*DPyP)]$_2$ (**13**), respectively.

When the coordination bonds that hold these assemblies together are both stable and inert, their formation from the components occurs under kinetic rather than thermodynamic control. By virtue of their thermodynamic and kinetic stability, some of these species can be further exploited as building blocks in the construction of higher order architectures through a hierarchical self-assembly approach (see for example the molecular sandwiches **19**–**21**). Through this modular approach, multi-chromophore assemblies become easily accessible with a relatively limited synthetic effort.

Even though solution spectroscopic measurements provide a wealth of information about the nature of the metal-mediated products, very often solid state X-ray structural determinations have proved to be essential for establishing the real composition and geometry of the multi-porphyrin assemblies. This is particularly true for highly symmetrical adducts. Indeed, we have contributed a remarkable number of X-ray structures to the still limited database of metal-mediated multi-porphyrin assemblies.

Some of the porphyrin assemblies, in particular those defining a cavity with specific shape and size, might behave as selective

hosts in molecular recognition reactions. Sensing properties, eventually leading to practical applications, may be found for the multi-porphyrins adducts in case their photophysical properties (e.g. their fluorescence) change as a result of molecular recognition. For example, molecular boxes **20** and **21** are particularly stimulating for further investigation, as they feature two cofacial porphyrins at a distance of about 11.4 Å (the bridging ligands) that might induce the inclusion of guest molecules of appropriate shape and size through π–π stacking interactions (e.g. aromatic hydrocarbons, aromatic bisimides, fullerenes).

Besides from the viewpoint of molecular architecture, the metal-mediated assemblies of porphyrins described in this review are of considerable interest in terms of their photophysical properties. Generally speaking, the assemblies are characterized by the occurrence of efficient intercomponent energy transfer processes. In the assemblies, the *direction* of energy flow is determined by the energy gradient between the excited states of the various chromophores. This can be conveniently programmed at the synthetic level by selective metalation of the various chromophoric units, as the energy levels of metal porphyrins are always higher than those of free-base porphyrins. The *type* of energy transfer can be further controlled by the metal used: with light metals such as Zn, singlet–singlet energy transfer is obtained; with heavy metals such as Ru, the energy transfer takes place at the triplet level. All these features make the metal-mediated assemblies of porphyrins interesting candidates for the design of artificial antenna systems.

A further dimension in the photophysics of metal-mediated assemblies can be added by substituting some of the porphyrin units with iso-structural perylene bisimide derivatives (e.g., 4′-*trans*DPyP with DPyPBI). Given the easy reduction of these units, new electron transfer pathways become available to the assemblies, in addition to the energy transfer ones. In perspective, this may permit the design of assemblies coupling both the antenna and charge separating functions.

In all cases, the intercomponent processes taking place in the metal-mediated assemblies are extremely fast, with time constants in the picosecond time domain. Therefore, extensive use of ultrafast techniques such as femtosecond pump-probe spectroscopy are required in the photophysical characterization of these systems. Thanks to the highly structured, specific spectra of the chromophores, not only kinetic information but also unambiguous qualitative identification of the intercomponent transfer processes is usually obtained.

Finally, despite the increased structural complexity, the photo-induced functions of elaborated artificial assemblies of chromophores are most often still far from those of natural systems. Nevertheless, a deep understanding of the construction and photophysical principles is crucial for a more appropriate choice of the building units for improving the photo-induced response of the assemblies. In addition, towards practical utilization, it would be appropriate to further organize a large number of functional systems into ordered structures. For example, functional multiporphyrin arrays might be anchored on solid surfaces, such as metals or wide band gap semiconductors, or on metal nanoparticles.

Acknowledgements

Acknowledgments are made for financial support to the donors of the Petroleum Research Fund, administered by the ACS (grant ACS PRF# 38892-AC3) and to MIUR (PRIN 2003 no. 2003035553 and FIRB-RBNE019H9K projects). Most of the X-ray structures mentioned or showed in this contribution were solved by Prof. Ennio Zangrando (Dipartimento di Scienze Chimiche, Università di Trieste), who also very kindly provided the new drawings.

References

[1] (a) V. Balzani, F. Scandola, Supramolecular Photochemistry, Horwood, Chichester, UK, 1991;
(b) V. Balzani, F. Scandola, in: J.L. Atwood, J.E.D. Davies, D.D. Mac Nicol, F. Vögtle, D.N. Reinhoudt (Eds.), Comprehensive Supramolecular Chemistry, vol. 10, Pergamon Press, Oxford, 1996.

[2] (a) J. Deisenhofer, O. Epp, K. Miki, R. Huber, H. Michel, J. Mol. Biol. 180 (1984) 385;
(b) J. Deisenhofer, O. Epp, I. Sinning, H. Michel, J. Mol. Biol. 246 (1995) 429;
(c) J.P. Allen, G. Feher, T.O. Yeates, H. Komiya, D.C. Rees, Proc. Natl. Acad. Sci. USA 84 (1987) 5730;
(d) A. Zouni, H.-T. Witt, J. Kern, P. Fromme, N. Krauss, W. Saenger, P. Orth, Nature 409 (2001) 739;
(e) K.N. Ferreira, T.M. Iverson, K. Maghlaoui, J. Barber, S. Iwata, Science 303 (2004) 1831;
(f) P. Jordan, P. Fromme, H.T. Witt, O. Klukas, W. Saenger, N. Krauss, Nature 411 (2001) 909.

[3] (a) R. van Grondelle, J.P. Dekker, T. Gillbro, V. Sundstrom, Biochim. Biophys. Acta 1187 (1994) 1;
(b) G. McDermott, S.M. Prince, A.A. Freer, A.M. Hawthornthwaite-Lawless, M.Z. Papiz, R.J. Cogdell, N.W. Isaacs, Nature 374 (1995) 517;
(c) W. Kuhlbrandt, Nature 374 (1995) 497;
(d) T. Pullerits, V. Sundström, Acc. Chem. Res. 29 (1996) 381;
(e) T. Ritz, S. Park, K. Schulten, J. Phys. Chem. B 105 (2001) 8259;
(f) M.Z. Papiz, S.M. Prince, T. Howard, R.J. Cogdell, N.W. Isaacs, J. Mol. Biol. 326 (2003) 1523.

[4] (a) M.R. Wasielewski, Chem. Rev. 92 (1992) 435;
(b) D. Gust, T.A. Moore, A.L. Moore, Acc. Chem. Res. 26 (1993) 198;
(c) A. Harriman, J.-P. Sauvage, Chem. Soc. Rev. 25 (1996) 41;
(d) I.M. Bennett, H.M. Vanegas Farfano, F. Bogani, A. Primak, P.A. Liddell, L. Otero, L. Sereno, J.J. Silber, A.L. Moore, T.A. Moore, D. Gust, Nature 420 (2002) 401;
(e) S.N. Smirnov, P.A. Liddell, I.V. Vlassiouk, A. Teslja, D. Kuciauskas, C.L. Braun, A.L. Moore, T.A. Moore, D. Gust, J. Phys. Chem. A 107 (2003) 7567;
(f) D.M. Guldi, Pure Appl. Chem. 75 (2003) 1069;
(g) S.L. Gould, G. Kodis, R.E. Palacios, L. de la Garza, A. Brune, D. Gust, T.A. Moore, A.L. Moore, J. Phys. Chem. B 108 (2004) 10566;
(h) B. Rybtchinski, L.E. Sinks, M.R. Wasielewski, J. Am. Chem. Soc. 126 (2004) 12268.

[5] (a) S. Anderson, H.L. Anderson, A. Bashall, M. McPartlin, J.K.M. Sanders, Angew. Chem. Int. Ed. Engl. 34 (1995) 1096;
(b) J. Davila, A. Harriman, L.R. Milgrom, Chem. Phys. Lett. 136 (1987) 427;
(c) S. Prathapan, T.E. Johnson, J.S. Lindsey, J. Am. Chem. Soc. 115 (1993) 7519;
(d) J.-S. Hsiao, B.P. Krueger, R.W. Wagner, T.E. Johnson, J.K. Delaney, D.C. Mauzerall, G.R. Fleming, J.S. Lindsey, D.F. Bocian, R.J. Donohoe, J. Am. Chem. Soc. 118 (1996) 11181;
(e) A. Nakano, A. Osuka, I. Yamazaki, T. Yamazaki, Y. Nishimura, Angew. Chem. Int. Ed. Engl. 37 (1998) 3023;
(f) D. Kuciauskas, P.A. Liddell, S. Lin, T.E. Johnson, S.J. Weghorn, J.S.

Lindsey, A.L. Moore, T.A. Moore, D. Gust, J. Am. Chem. Soc. 121 (1999) 8604;
(g) H.L. Anderson, Chem. Commun. (1999) 2323;
(h) Y.H. Kim, D.H. Jeong, D. Kim, S.C. Jeoung, H.S. Cho, S.K. Kim, N. Aratani, A. Osuka, J. Am. Chem. Soc. 123 (2001) 76;
(i) S.I. Yang, S. Prathapan, M.A. Miller, J. Seth, D.F. Bocian, J.S. Lindsey, D. Holten, J. Phys. Chem. B 105 (2001) 8249;
(j) M. Taniguchi, D. Ra, C. Kirmaier, E.K. Hindin, J.K. Schwartz, J.R. Diers, D.F. Bocian, J.S. Lindsey, R.S. Knox, D. Holten, J. Am. Chem. Soc. 125 (2003) 13461;
(k) R. Takahashi, Y. Kobuke, J. Am. Chem. Soc. 125 (2003) 2372;
(l) T.S. Balaban, A.D. Bhise, M. Fischer, M. Linke-Schaetzel, C. Roussel, N. Vanthuyne, Angew. Chem. Int. Ed. 42 (2003) 2140;
(m) X. Pen, T. Aratani, T. Matsumoto, T. Kawai, I.-W. Hwang, T.K. Ahn, D. Kim, A. Osuka, J. Am. Chem. Soc. 126 (2004) 4468.

[6] (a) J.-C. Chambron, V. Heitz, J.-P. Sauvage, in: K.M. Kadish, K.M. Smith, R. Guillard (Eds.), The Porphyrin Handbook, vol. 6, Academic Press, 2000 (Chapter 40);
(b) J. Wojaczyński, L.-L. Grażyńsky, Coord. Chem. Rev. 204 (2000) 113;
(c) T. Imamura, K. Fukushima, Coord. Chem. Rev. 198 (2000) 133.

[7] (a) C.M. Drain, J.-M. Lehn, J. Chem. Soc., Chem. Commun. (1994) 2313;
(b) H. Yuan, L. Thomas, L.K. Woo, Inorg. Chem. 35 (1996) 2808;
(c) P.J. Stang, J. Fan, B. Olenyuk, Chem. Commun. (1997) 1453;
(d) C.M. Drain, F. Nifiatis, A. Vasenko, J.D. Batteas, Angew. Chem. Int. Ed. Engl. 37 (1998) 2344;
(e) J. Fan, J.A. Whiteford, B. Olenyuk, M.D. Levin, P.J. Stang, E.B. Fleischer, J. Am. Chem. Soc. 121 (1999) 2741;
(f) M.M. Schmitz, S. Leininger, T. Fan, A.M. Arif, P.J. Stang, Organometallics 18 (1999) 4817;
(g) E. Iengo, B. Milani, E. Zangrando, S. Geremia, E. Alessio, Angew. Chem. Int. Ed. 39 (2000) 1096;
(h) K.E. Splan, M.H. Keefe, A.M. Massari, K.A. Walters, J.T. Hupp, Inorg. Chem. 41 (2002) 619, and references therein;
(i) E. Iengo, E. Zangrando, M. Bellini, R. Alessio, A. Prodi, C. Chiorboli, F. Scandola, Inorg. Chem. 44 (2005) 9752.

[8] (a) C.V.K. Sharma, G.A. Broker, J.G. Huddleston, J.W. Baldwin, R.M. Metzger, R.D. Rogers, J. Am. Chem. Soc. 121 (1999) 1137;
(b) L. Pan, B.C. Nool, X. Wang, Chem. Commun. (1999) 157.

[9] (a) A. Prodi, M.T. Indelli, C.J. Kleverlaan, F. Scandola, E. Alessio, T. Gianferrara, L.G. Marzilli, Chem. Eur. J. 5 (1999) 2668;
(b) E. Alessio, S. Geremia, S. Mestroni, E. Iengo, I. Srnova, M. Slouf, Inorg. Chem. 38 (1999) 869;
(c) E. Alessio, S. Geremia, S. Mestroni, T. Gianferrara, M. Slouf, A. Prodi, Inorg. Chem. 38 (1999) 2527;
(d) A. Prodi, M.T. Indelli, C.J. Kleverlaan, E. Alessio, F. Scandola, Coord. Chem. Rev. 229 (2002) 51.

[10] (a) K. Funatsu, A. Kimura, T. Imamura, A. Ichimura, Y. Sasaki, Inorg. Chem. 36 (1997) 1626;
(b) N. Kariya, T. Imamura, Y. Sasaki, Inorg. Chem. 37 (1998) 1658;
(c) K. Funatsu, T. Imamura, A. Ichimura, Y. Sasaki, Inorg. Chem. 37 (1998) 1798;
(d) H. Shinmori, T. Kajiwara, A. Osuka, Tetrahedron Lett. 42 (2001) 3617;
(e) T.S. Balaban, R. Goddard, M. Linke-Schaetzel, J.-M. Lehn, J. Am. Chem. Soc. 125 (2003) 4233;
(f) A. Tsuda, S. Sakamoto, K. Yamaguchi, T. Aida, J. Am. Chem. Soc. 125 (2003) 15722;
(g) M. Vinodu, I. Goldberg, Inorg. Chem. 43 (2004) 7582.

[11] G. Orlandi, S. Monti, F. Barigelletti, V. Balzani, Chem. Phys. 52 (1980) 313.

[12] Z. Murtaza, A.P. Zipp, L.A. World, D. Graff, W.E. Jones Jr., W.D. Bates, T.J. Meyer, J. Am. Chem. Soc. 113 (1991) 5113.

[13] K.R. Naqvi, C. Steel, Spectrosc. Lett. 26 (1993) 1761.

[14] M.E. Sigman, G.L. Closs, J. Phys. Chem. 95 (1991) 5012.

[15] D.B. MacQueen, J.R. Eyler, K.S. Schanze, J. Am. Chem. Soc. 114 (1992) 1897.

[16] A.A. Lamola, in: A.A. Lamola, N.J. Turro (Eds.), Energy Transfer and Organic Photochemistry, Wiley/Interscience, 1969.

[17] N.J. Turro, Modern Molecular Photochemistry, University Science Books, Mill Valley, CA, 1991.

[18] G.D. Scholes, K.P. Ghiggino, A.M. Oliver, M.N. Paddon-Row, J. Phys. Chem. 97 (1993) 11871.

[19] H. Oevering, J.W. Verhoeven, M.N. Paddon-Row, E. Cotsaris, N.S. Hush, Chem. Phys. Lett. 143 (1988) 488.

[20] G.L. Closs, P. Piotrowiak, J.M. McInnis, G.R. Fleming, J. Am. Chem. Soc. 110 (1988) 2652.

[21] G.L. Closs, M.D. Johnson, J.R. Miller, P. Piotrowiak, J. Am. Chem. Soc. 111 (1989) 3751.

[22] A. Weller, Z. Phys. Chem. 133 (1982) 93.

[23] R.A. Marcus, Annu. Rev. Phys. Chem. 15 (1964) 155.

[24] N. Sutin, Prog. Inorg. Chem. 30 (1983) 441.

[25] R.A. Marcus, N. Sutin, Biochim. Biophys. Acta 811 (1985) 265.

[26] J. Jortner, J. Chem. Phys. 64 (1976) 4860.

[27] J. Ulstrup, Charge Transfer Processes in Condensed Media, Springer Verlag, Berlin, 1979.

[28] J.R. Miller, J.V. Beitz, R.K. Huddleston, J. Am. Chem. Soc. 106 (1984) 5057.

[29] T.J. Meyer, H. Taube, in: S.J. Wilkinson, R.D. Gillard, J.A. McCleverty (Eds.), Comprehensive Coordination Chemistry, vol. 1, Pergamon Press, Oxford, 1987.

[30] M.D. Newton, Chem. Rev. 91 (1991) 767.

[31] H. Oevering, J.W. Verhoeven, M.N. Paddon-Row, J.M. Warman, Tetrahedron 45 (1989) 4751.

[32] J. Halpern, L.E. Orgel, Discuss. Faraday Soc. 29 (1960) 32.

[33] H.M. McConnell, J. Chem. Phys. 35 (1961) 508.

[34] B. Mayoh, P. Day, J. Chem. Soc., Dalton (1974) 846.

[35] J.R. Miller, J.V. Beitz, J. Chem. Phys. 74 (1981) 6746.

[36] D.E. Richardson, H. Taube, J. Am. Chem. Soc. 10 (1983) 540.

[37] M.N. Paddon-Row, in: V. Balzani (Ed.), Electron Transfer in Chemistry, vol. III, Wiley/VCH, Weinheim, 2001 (Chapter 2.3).

[38] F. Scandola, C. Chiorboli, M.T. Indelli, M.A. Rampi, V. Balzani (Eds.), Electron Transfer in Chemistry, vol. III, Wiley/VCH, Weinheim, 2001 (Chapter 2.1).

[39] G.L. Closs, J.R. Miller, Science 240 (1988) 440.

[40] I.R. Gould, J.E. Moser, B. Armitage, S. Farid, J. Am. Chem. Soc. 111 (1989) 1917.

[41] The 2′ position cannot be easily exploited for coordination due to steric reasons.

[42] (a) E. Alessio, M. Macchi, S. Heath, L.G. Marzilli, Chem. Commun. (1996) 1411;
(b) E. Alessio, E. Iengo, L.G. Marzilli, Supramol. Chem. 14 (2002) 103.

[43] E. Iengo, E. Zangrando, S. Mestroni, G. Fronzoni, M. Stener, E. Alessio, J. Chem. Soc., Dalton Trans. (2001) 1338.

[44] A. Prodi, C. Chiorboli, F. Scandola, E. Iengo, E. Alessio, R. Dobrawa, F. Würthner, J. Am. Chem. Soc. 127 (2005) 1454.

[45] (a) E. Alessio, G. Mestroni, G. Nardin, W.M. Attia, M. Calligaris, G. Sava, S. Zorzet, Inorg. Chem. 27 (1988) 4099;
(b) E. Alessio, B. Milani, M. Bolle, G. Mestroni, P. Faleschini, S. Geremia, M. Calligaris, Inorg. Chem. 34 (1995) 4722.

[46] (a) E. Alessio, M. Macchi, S.L. Heath, L.G. Marzilli, Inorg. Chem. 36 (1997) 5614;
(b) E. Iengo, E. Zangrando, E. Alessio, Eur. J. Inorg. Chem. (2003) 2371.

[47] E. Iengo, E. Zangrando, R. Minatel, E. Alessio, J. Am. Chem. Soc. 124 (2002) 1003.

[48] E. Iengo, E. Zangrando, S. Geremia, R. Graff, B. Kieffer, E. Alessio, Chem. Eur. J. 8 (2002) 4670.

[49] (a) Y. Kokube, H. Miyaji, Bull. Chem. Soc. Jpn. 69 (1996) 3563;
(b) U. Michelsen, C.A. Hunter, Angew. Chem. Int. Ed. 39 (2000) 764;
(c) C.A. Hunter, L.D. Sarson, Angew. Chem. Int. Ed. Engl. 33 (1994) 2313;
(d) R.T. Stibrany, J. Vasudevan, S. Knapp, J.A. Potenza, T. Emge, H.J. Sugar, J. Am. Chem. Soc. 118 (1996) 3980;

(e) A.K. Burrell, D.L. Officer, D.C.W. Reid, K.Y. Wild, Angew. Chem. Int. Ed. 37 (1998) 114;
(f) K. Funatsu, A. Kimura, T. Imamura, Y. Sasaki, Chem. Lett. (1995) 765.
[50] (a) K. Ogawa, Y. Kobuke, Angew. Chem. Int. Ed. 39 (2000) 4070;
(b) K. Ogawa, T. Zhang, K. Yoshihara, Y. Kobuke, J. Am. Chem. Soc. 124 (2002) 22;
(c) D. Furutsu, A. Satake, Y. Kobuke, Inorg. Chem. 44 (2005) 4460;
(d) R. Takahashi, Y. Kobuke, J. Org. Chem. 70 (2005) 2745.
[51] (a) H.L. Anderson, C.A. Hunter, M.N. Meah, J.K.M. Sanders, J. Am. Chem. Soc. 112 (1990) 5780;
(b) H.L. Anderson, S. Anderson, J.K.M. Sanders, J. Chem. Soc., Perkin Trans. 1 (1995) 2231;
(c) C.J. Chang, Y. Deng, A.F. Heyduk, C.K. Chang, D.G. Nocera, Inorg. Chem. 39 (2000) 959;
(d) K. Tashiro, Y. Hirabayashi, T. Aida, K. Saigo, K. Fujiwara, K. Komatsu, S. Sakamoto, K. Yamaguchi, J. Am. Chem. Soc. 124 (2002) 12086.
[52] A. Prodi, C.J. Kleverlaan, M.T. Indelli, F. Scandola, E. Alessio, E. Iengo, Inorg. Chem. 40 (2001) 3498.
[53] C. Chiorboli, Unpublished results.
[54] D.M. Guldi, T. Da Ros, P. Braiuca, M. Prato, E. Alessio, J. Mater. Chem. 12 (2002) 2001.
[55] J. Salbeck, H. Kunkely, H. Langhals, R.W. Saalfrank, J. Daub, Chimia 43 (1989) 6.
[56] F. Würthner, Chem. Commun. (2004) 1564.
[57] A. Prodi, C. Chiorboli, F. Scandola, E. Iengo, E. Alessio, submitted for publication.